

Key Points:

- Six types of typical chlorophyll patterns on mesoscale eddies and their submesoscale fine-structures are identified globally by artificial intelligence (AI) method
- The typical patterns tend to substantially enhance chlorophyll concentration of the corresponding eddies
- The wave-number spectral slope of the typical chlorophyll pattern is significantly different from the background value

Supporting Information:

Supporting Information may be found in the online version of this article.

Correspondence to:

Z. Zhang,
zhengguang@ouc.edu.cn

Citation:

Nian, R., Yuan, M., Zhang, Z., Wu, T., Ji, Y., Wang, Y., et al. (2024). Different types of surface chlorophyll patterns of oceanic mesoscale eddies identified by AI framework. *Journal of Geophysical Research: Oceans*, 129, e2024JC021176. <https://doi.org/10.1029/2024JC021176>

Received 3 APR 2024

Accepted 4 SEP 2024

Author Contributions:

Conceptualization: Rui Nian, Zhengguang Zhang

Data curation: Minghan Yuan, Hua Yang, Hengfu Xu

Formal analysis: Rui Nian, Minghan Yuan, Zhengguang Zhang, Tong Wu, Hua Yang

Funding acquisition: Rui Nian, Zhengguang Zhang

Investigation: Rui Nian, Zhengguang Zhang, Yajie Ji, Yanmei Wang, Hua Yang, Kexin Shi

Methodology: Rui Nian, Minghan Yuan, Zhengguang Zhang

Project administration: Rui Nian, Zhengguang Zhang

Resources: Rui Nian, Zhengguang Zhang

Software: Minghan Yuan, Tong Wu, Hua Yang, Zhen Fu, Hengfu Xu

Different Types of Surface Chlorophyll Patterns of Oceanic Mesoscale Eddies Identified by AI Framework

Rui Nian¹ , Minghan Yuan¹ , Zhengguang Zhang^{2,3} , Tong Wu¹, Yajie Ji¹, Yanmei Wang¹, Hua Yang¹, Zhen Fu¹, Hengfu Xu¹, Kexin Shi⁴, and Bo He¹

¹School of Electronic Engineering, Ocean University of China, Qingdao, China, ²Frontiers Science Center for Deep Ocean Multispheres and Earth System (FDOMES) and Key Laboratory of Physical Oceanography, Ocean University of China, Qingdao, China, ³Laoshan Laboratory, Qingdao, China, ⁴China United Network Communications Co., Ltd., Qingdao, China

Abstract Oceanic mesoscale eddies (with scale $10^1\text{--}10^2$ km) and their submesoscale fine structures (with scale $10^0\text{--}10^1$ km) can effectively induce vertical motions and bring nutrients into the oceanic euphotic layer, which leaves abundant footprints on the ocean surface chlorophyll distributions and have the potential to promote primary productivity of oceanic ecosystem. In return, these surface chlorophyll footprints observed by ocean color satellites can serve as a useful tool to reveal the spatial structures of mesoscale eddies and their submesoscale fine structures. By combining artificial intelligence (AI) algorithms to develop a series of identification strategies for typical surface chlorophyll patterns around mesoscale eddies, we find that over 20% of mesoscale eddy observations exhibit identifiable typical chlorophyll patterns, which tends to regulate an increase of the surface chlorophyll concentration within the corresponding eddies, especially enhancing by about 30% in nutrient-restricted subtropical regions compared with the background values. Based on their geometric features, typical chlorophyll patterns are primarily classified as Core, Spiral, Tail, Ring, Loop, and Eye respectively by clustering algorithm. Further spatial-spectral analysis found that the typical patterns on eddies exhibit a much steeper wave-number spectral slope about -3 , compared to the non-typical distributions on eddies and the non-eddy background distribution (about $-2.7\text{--}-2.2$). This implies that the occurrence of different typical chlorophyll patterns may correspond to specific mesoscale and submesoscale dynamic processes.

Plain Language Summary Mesoscale eddies and their submesoscale fine structures collectively play non-negligible roles in sustaining nutrient supply and promoting productivity in the oceanic euphotic layer. Although submesoscale processes are believed to result in ageostrophic motions and allow forward oceanic energy cascade, the resolutions of traditional in-situ ocean measurements and satellite altimetry observations are typically too coarse to resolve them. In this paper, we elaborate on artificial intelligence (AI) techniques to develop a series of typical surface chlorophyll pattern identification strategies. The AI framework automatically identified six types of typical chlorophyll patterns of mesoscale eddy, in the context of the generally comparable geometric characteristics that are potentially reflected from their underlined oceanic dynamics. Over 20% mesoscale eddy observations tend to exhibit identifiable typical chlorophyll patterns, which leads to a remarkable increase of surface chlorophyll concentration. The wave-number spectrum of eddy-induced typical patterns exhibit a significantly steeper slope, in comparison of the non-typical distributions on eddies and the non-eddy background distribution. Our results may help to establish parameterizations for the submesoscale processes of mesoscale eddies, or provide an observational baseline to verify high-resolution physical-biogeochemical coupled oceanic numerical models, or even improve the model simulations of oceanic primary productivity and carbon fixation capacity.

1. Introduction

Oceanic mesoscale eddies, with a radius of approximately 10^2 km and temporal scales from weeks to months, account for 80%–90% of the kinetic energy in the world's oceans (Chelton et al., 2011; Falkowski et al., 1991; Ferrari & Wunsch, 2009; Q. He et al., 2024; Martínez-Moreno et al., 2021; McGillicuddy et al., 1998, 2003, 2007; Nian et al., 2021; Oschlies & Garçon, 1998; Pascual et al., 2006; Wunsch, 2007; Zhang & Qiu, 2020). Mesoscale eddies play a crucial role in the energy balance of the ocean, serve as a principal sink for the energy of planetary-scale mean oceanic circulation through balanced instabilities, such as the quasi-geostrophic barotropic and baroclinic instabilities (Vallis, 2006), and constitute a pivotal component in the entire oceanic energy cascade

Supervision: Rui Nian,
Zhengguang Zhang, Yajie Ji,
Yanmei Wang

Validation: Tong Wu, Yajie Ji,
Yanmei Wang, Kexin Shi

Visualization: Minghan Yuan, Tong Wu,
Zhen Fu, Kexin Shi, Bo He

Writing – original draft: Rui Nian,
Minghan Yuan, Zhengguang Zhang,
Tong Wu, Yajie Ji, Yanmei Wang,
Hua Yang

Writing – review & editing: Rui Nian,
Minghan Yuan, Zhengguang Zhang,
Yajie Ji, Yanmei Wang

chain. The energy in the oceanic dynamical system primarily originates from large-scale forcing, such as wind and solar radiation, while energy dissipation is mainly achieved by small-scale oceanic turbulence motions (Du et al., 2021; Elistratov et al., 2020; Hu et al., 2021; Pérez & Calil, 2017). To maintain energy balance, the oceanic dynamical system needs to transfer energy from large-scale to small-scale through forward energy cascade, satisfying the energy consumption requirements (Sasaki et al., 2014; Schubert et al., 2020; Vallis, 2006). However, mesoscale eddies are generally considered to approximately satisfy geostrophic balance, and the corresponding quasi-geostrophic dynamics exhibit an inverse energy cascade, meaning that energy is transferred from smaller to larger scales, failing to provide an effective energy pathway to smaller scales and address the overall energy balance in the ocean. The central issue is how to overcome the constraints of geostrophic balance and effectively transfer energy to smaller scales (Qiu et al., 2017, 2018). It has been progressively realized that the ageostrophic components of submesoscale motions play an important role in this forward energy cascade.

The submesoscale flow has a horizontal scale of approximately 10^0 – 10^1 km and a time scale of 1–10 days (Lévy et al., 2012; Mahadevan, 2016; Ni et al., 2021). Submesoscale processes emerge from instability processes which break the geostrophic balance, thus characterized by smaller scales than mesoscale eddies and significant ageostrophic components (Capet et al., 2008; McWilliams, 2016). These instability processes also facilitate forward energy cascade, enabling the energy transfer from mesoscale to submesoscale (Capet et al., 2008; McWilliams, 2016). Great efforts have been given to study the instability mechanisms that give rise to submesoscale phenomena, such as frontogenesis (Hoskins, 1982; Hoskins & Bretherton, 1972), mixed-layer instability processes (Boccaletti et al., 2007; Colas et al., 2013; Fox-Kemper et al., 2008), symmetric instability processes (Bachman et al., 2017; Bachman & Taylor, 2014; Bennetts & Hoskins, 1979; Haine & Marshall, 1998; Jing et al., 2021; Thomas et al., 2013), anticyclonic-ageostrophic instability (McWilliams, 2008; McWilliams & Yavneh, 1998; Molemaker et al., 2005). The submesoscale ageostrophic motions are dynamically important as they determine the equilibrium state of oceanic dynamic system by releasing the available energy contained within mesoscale balanced motions (Zhang & Qiu, 2018).

On the other hand, the ageostrophic motions break geostrophic balance and can induce significant vertical flow, which may transport nutrients into the euphotic layer. Mesoscale eddies and their submesoscale fine structures have been progressively recognized as having considerable contribution in supplying nutrients and supporting global oceanic primary productivity (Mahadevan, 2016; McGillicuddy et al., 2007; McWilliams, 2010; Ni et al., 2021; Zhang et al., 2018; Zhang & Qiu, 2020), which has a potentially impact on the ocean's carbon fixation capacity under global warming (Guo et al., 2019; Zhang et al., 2019). When the vertical motions of mesoscale eddies and their submesoscale fine structures supply nutrients to the euphotic layer, they promoting the growth of surface chlorophyll and leave footprints on the surface chlorophyll concentration distributions, which can be observed by high-resolution ocean color remote sensing. Although the instability processes provide a variety of physical mechanisms that generate ageostrophic perturbations, the dynamical definitions of the resulted submesoscale fine structures of mesoscale eddies remain obscure and can not be solely explained by the instability processes. In fact, even all the types of these fine structures on mesoscale eddies have not been fully understood and classified completely, which largely due to the observational challenges and difficulties posed by the shorter spatiotemporal scales of the submesoscale.

The resolutions of traditional in-situ ocean measurements and satellite altimetry observations are typically too coarse to resolve these small-scale and short-lifetime of submesoscale processes. One possible way to overcome this obstacle is to utilize other satellite remote sensing data, such as sea surface temperature (SST) and near-surface chlorophyll, which is available at high resolution (~ 4 km) and global coverage (Buckingham et al., 2017; Liu et al., 2014; Munk et al., 2000; Ni et al., 2021). The surface chlorophyll footprints could reveal the horizontal fine structures of mesoscale eddies and their submesoscale processes in the satellite remote-sensing ocean color maps. One of the most typical fine structures of vortex is the spiral band around the vortex center, for example, the spiral arms of the galaxy in the universe or the spiral rain band of the tropical cyclone in the atmosphere (Lin & Lau, 1979; Montgomery & Kallenbach, 1997). For oceanic mesoscale eddies, the spiral bands with high surface chlorophyll concentration are also commonly observed by ocean color satellite. These spiral chlorophyll bands on the mesoscale eddies have been globally identified and systematically investigated, and further diagnosis indicates that they are likely caused by a particular type of submesoscale process on mesoscale eddies, which can be dynamically explained by the vortex Rossby waves (Zhang & Qiu, 2020). Other fine structures of mesoscale eddies, for example, Chlorophyll Rings (CRs), have also been identified by using satellite observations of near-surface chlorophyll concentration (Xu et al., 2019).

These fine structures of mesoscale eddies can be referred as certain types of oceanic submesoscale features (Chelton et al., 2011; Gaube et al., 2013, 2014, 2015; Q. He et al., 2016; McGillicuddy, 2016). In order to interpret the underlying dynamic processes, it is necessary to identify all possible types of these fine structures. This puts a major challenge to the existing methods commonly designed to identify single type of spatial pattern, due to the difficulties in simultaneously retrieving, classifying, and validating enormous amount of observations. Consequently, so far, there is still a lack of surveys that could be statistically and systematically conducted to identify all the emerging chlorophyll patterns from the overall mesoscale eddies and their submesoscale fine structures on a global scale, due to the absence of efficient means capable of massively unbiased identification.

Recently, owing to the great success of deep learning, all kinds of most emerging and advanced artificial intelligence (AI) algorithms have been developed and made progresses in the context (Kalvankar et al., 2020), in learning the deterministic spatial correlations and temporal dependencies, from Deep Belief Networks (DBN) (Hinton et al., 2006), Deep Convolutional Neural Networks (CNN) (Karpathy et al., 2014), Generative Adversarial Networks (GAN) (Goodfellow et al., 2014), Deep Residual Networks (ResNet) (K. He et al., 2016), to the recent Transformer (Vaswani et al., 2017), MobileNets (Howard et al., 2017; Sandler et al., 2018), EfficientNets (Tan & Le, 2019, 2021), Swin-Transformers (Liu et al., 2021, 2022). A CNN model was proposed for multi-year ENSO forecasts using physically reasonable precursors (Ham et al., 2019). This model outperformed most of the current state-of-the-art dynamical forecasts with the all-season correlation skill of the Niño3.4 index for lead times of up to one and a half years, and also predicted the detailed zonal distribution of sea surface temperatures. A global oceanic eddy identification mechanism was developed with CNN and extreme gradient boosting, recapturing 36% of eddies with 98% accuracy by extracting the representative vertical features from 18-year Argo data, demonstrating the potentials of the proposed method in identifying eddies (Chen et al., 2021). An enhanced MIM strategy was put forward for mesoscale eddy prediction, equipped with a Gated Recurrent Unit (GRU) and a spatial attention module in a scheduled sampling manner (Nian et al., 2021). This strategy complements to strengthen spatio-temporal nonstationary features for long-term dependencies from SLA time series, benefiting the predictability of mesoscale eddies and the deployment of glider, AUV, and other observational platforms. A multi-task machine learning model was presented for the multi-seasonal long-term prediction of the Indian Ocean Dipole (IOD), which could help assess the importance among predictors and improve the IOD prediction performances well up to a 7-month lead, compared to most world-class dynamical models (Ling et al., 2022). Among them, EfficientNets revolutionarily exploit a family of convolutional networks that uniformly balance all dimensions of depth, width, resolution by neural architecture search (NAS), which enables to produce all kinds of baseline models via a simple yet highly effective compound scaling coefficient, surpassing most of the state-of-the-art accuracy with an order of magnitude fewer parameters and Floating Point Operations (FLOPs). However, it is still of great challenges to distinguish the suitable versions of identification strategies for all possible types of the fine structures of mesoscale eddies, due to the strong nonlinearity degrees and high-order non-stationarity from eddy-induced variation in geometric shapes, sizes, strengths, and life cycles. Attention-based methods show great potential in performance improvement, it can be integrated into any CNN architectures seamlessly with negligible overheads and is end-to-end trainable along with base CNNs, which bring clear performance gain for various deep CNN architectures (Gao et al., 2019; Roy et al., 2018; Wang et al., 2020; Woo et al., 2018).

This study integrates chlorophyll satellite ocean color remote sensing data to develop a deep learning-based algorithm for the identification and classification of typical chlorophyll patterns at ocean surface. The recognition algorithm is applied to identify typical chlorophyll patterns induced by mesoscale eddies and their fine structures in global sea surface chlorophyll data from 1998 to 2017. Subsequently, a clustering algorithm is employed to chlorophyll distribution around mesoscale eddies, and six types of typical chlorophyll patterns of mesoscale eddies are identified and classified globally as Core, Spiral, Tail, Eye, Loop, and Ring respectively. The identified typical patterns tend to enhance chlorophyll concentration globally, especially in subtropical regions, at the same time, this enhancing effect exhibits certain seasonality. The data and method used in this study is introduced in Section 2, the deep learning-based recognition and clustering algorithms are described in detailed. The corresponding analysis results of these typical chlorophyll patterns are presented in Section 3, including their influences on surface chlorophyll concentration and their wave-number spectral slope. The summary and discussion are given in the final section.

2. Data and Methods

2.1. Chlorophyll Data

The chlorophyll product in our study, is retrieved from European Space Agency (ESA) GlobColour Project (<https://globcolour.info>), with a long daily time-series of consistently calibrated global ocean color information of the best possible coverage at a spatial resolution of 4 km from 1998 to 2017 (Maritorena et al., 2010; Maritorena & Siegel, 2005), by merging three most capable sensors SeaWiFS (SeaStar), MODIS (Aqua) and MERIS (Envisat). Surface chlorophyll data provides a proxy for phytoplankton biomass (Travers-Smith et al., 2021). The unit for chlorophyll concentration is mg/m³, and all chlorophyll values in this study are expressed by their Base-10 logarithm *Chl*. In order to achieve sufficient data coverage, the chlorophyll data *Chl* is averaged within a time window [t_0-3, t_0+3] (Zhang & Qiu, 2020).

2.2. Mesoscale Eddy Trajectory Atlas Product

The Mesoscale Eddy Trajectory Atlas Product META2.0 DT was produced by SSALTO/DUACS and distributed by AVISO+ (<https://aviso.altimetry.fr>) with support from Center National d'Etudes Spatiales (CNES). The coverage region of the satellite multimission altimetry for the product reaches the global scope, with the spatial resolution $0.25^\circ \times 0.25^\circ$ and the temporal resolution daily, from January 1993 to March 2020. A total of 281,254 mesoscale eddy trajectories were detected and tracked in the global ocean, providing with the polarity, location (x_c, y_c), amplitude A_0 , radius R_0 , tangential rotation velocity V_{adv} , and associated metadata, from an automatic eddy identification and tracking algorithm (Chelton et al., 2011; Pegliasco et al., 2022).

2.3. Overall Framework for Typical Chlorophyll Pattern Identification

Typical surface chlorophyll patterns are footprints of mesoscale eddies and their submesoscale fine structures. In this paper, we make an attempt to develop a series of typical surface chlorophyll pattern identification strategies via EfficientNetV2 (Tan & Le, 2021), combined with weight guidance and salient pattern feedback, which quantifies to converge at similarity loss, label inference loss, as well as mutual information loss. The overall identification framework is composed of several correlative steps, including the eddy-induced chlorophyll distribution search, the typical chlorophyll pattern recognition, and the clustering of different types of typical patterns, as is shown in Figure 1. First, the original global chlorophyll data would be obtained around individual mesoscale eddy observations, and projected to an normalized eddy center coordinates (Zhang & Qiu, 2020). For a given mesoscale eddy observation, let its central location be (x_c, y_c) and the radius be R_0 at the time t_0 , the surface chlorophyll distribution can be projected into an eddy-centered coordinate (x_e, y_e) , with $x_e = x - x_c$ and $y_e = y - y_c$, and further normalized from its eddy radius as (x_n, y_n) by a horizontal scaling, with $x_n = x_e/R_0$, $y_n = y_e/R_0$, where x and y refer to the latitude and longitude coordinates of any specific data point in the sea surface chlorophyll distribution.

In our study, a total of 2,954,790 eddy observations collected from year 1998–2017 in the trajectory atlas, are retrieved to project surface chlorophyll distributions globally, which are inscribed within a search window of 2.5 times eddy radius by their normalized eddy center coordinates. Considering the data gaps due to the resulting quality degradation of the chlorophyll maps from the irregular tracks, swaths, sun glint and cloud cover (Maritorena & Siegel, 2005), a total of 922,682 eddy observations, with only surface chlorophyll distribution $Chl(x_n, y_n)$ up to over 90% of non-NAN values, are seen as the sufficient coverage and adopted in the following analysis. Additionally, 20,000 representative chlorophyll distribution samples are randomly and uniformly selected, to help ease the overfitting problem and promote the generalization capabilities in the model construction, configuration, selection, transfer learning during our identification process. A preliminary two-stage screening mechanism is applied to potentially assign a set of similar and comparable chlorophyll distribution samples into distinct, non-overlapping, mutually disjoint clusters, regardless the manual labeling, so as to automatically distinguish the most typical eddy-induced patterns that most explicitly exhibit footprints of mesoscale eddies from the rest of the samples in an unsupervised learning manner. One type of 50-layer residual neural network ResNet50 (K. He et al., 2016) is established as an auto-encoder to conduct feature mapping with residual learning and skip connections at a considerably increased depth for 20,000 randomly selected chlorophyll distribution samples. This process explicitly reformulates layers as learning residual functions with reference to layer inputs, instead of learning unreference functions, which performs to ease the optimization in a substantially deeper architecture, by a small amount of computation during training. The outputs of the encoder in ResNet50 is then utilized as the inputs

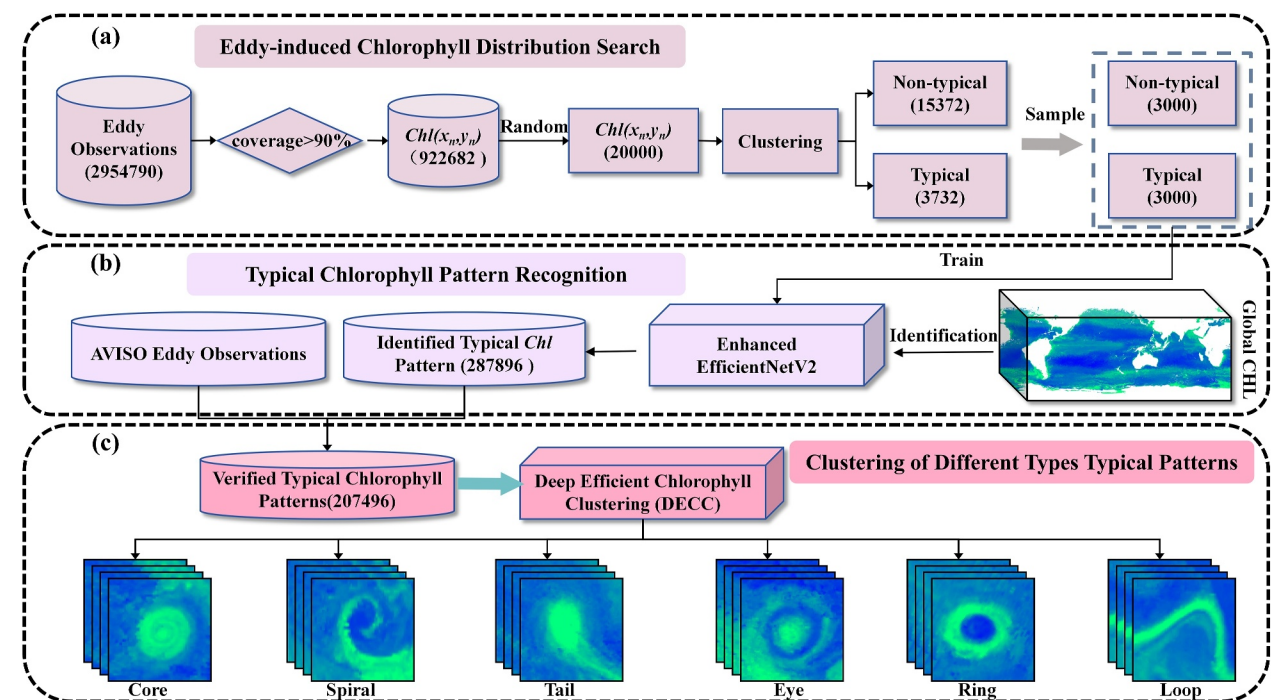


Figure 1. The overall framework of typical chlorophyll pattern identification. (a) Eddy-induced chlorophyll patterns search process in pink, including the chlorophyll distribution segments of global eddy observations retrieved from the trajectory atlas, the resulting chlorophyll maps with quality control of 90% coverage rate, the uniform sampling of representative chlorophyll samples, the preliminary clustering of the typical and non-typical chlorophyll patterns, the training set construction for recognition. (b) Typical chlorophyll pattern recognition process in purple, including the training in an EfficientNetV2 backbone, the inference to global typical chlorophyll patterns, the alignment toward all the existing eddy trajectories in atlas. (c) The clustering process of different types of the chlorophyll distributions around mesoscale eddies in peach-red, where the verified typical chlorophyll distribution patterns would be classified in an unsupervised manner by our proposed DECC.

for the conventional K-means clustering, through the dimensionality reduction to the representative chlorophyll distribution samples. The clusters of both typical and non-typical eddy-induced chlorophyll patterns would be further comprehensively determined in terms of similarity metrics, by the spatial distance measurement between the cluster centers and the encoded chlorophyll distribution features in a much lower dimension. Afterward, in each cluster, we perform a data cleaning step to remove those unusual chlorophyll distribution samples that are not normally distributed and lying extremely far away from the majority of the members, ahead of recognition network, resulting in 3,732 typical and 15,372 non-typical chlorophyll patterns.

In view of the sample distribution imbalance, we further randomly allocate 3,000 typical positive samples and 3,000 non-typical negative samples to fulfill the globally typical chlorophyll pattern recognition tasks during training, so as to alleviate the possible learning bias toward the majority of existing non-typical samples. We develop one enhanced EfficientNetV2 mechanism, with both Chlorophyll Critical Feature Weight Guidance Unit (CFG) and Chlorophyll Pattern Salient Feedback Unit (CSF) equipped, which makes a trade-off between model complexity and prediction accuracy for chlorophyll distributions highly associated with spatio-temporal variability of mesoscale eddies. A stochastic gradient descent (SGD) (Ruder, 2016) based algorithm (Adam Optimizer) is used to optimize the model by a cross-entropy loss function (Quinlan, 1993). In this way, an optimized recognition model is learned and tuned, which can be potentially applied to handle the common classification problem of global chlorophyll time series within a given sliding window for all the eddy trajectories, discriminating out a total of 287,896 typical chlorophyll patterns associated with mesoscale eddies and their fine structures. The central locations of all the above estimated typical chlorophyll patterns learned in this recognition model are aligned onto eddy centers retrieved from the trajectory atlas product as references, and a total of 207,496 eddy observations has been consistently identified, with regard to a valid eddy-induced overlapping within a frame of chlorophyll distribution toward the individual eddy center known in the atlas. Finally, these 207,496 eddy observations with the verified typical chlorophyll patterns are completely fed into one deep-learning based clustering model we developed, called Deep Efficient Chlorophyll Clustering (DECC), which

further automatically reveals six potential types of the existing typical chlorophyll distribution patterns, namely Core, Spiral, Tail, Eye, Ring, Loop, in the context of the generally comparable geometric characteristics reflected by their underlined oceanic dynamics.

2.4. Design of Typical Chlorophyll Pattern Clustering

In our study, we innovatively design one end-to-end unsupervised learning scheme for typical chlorophyll patterns, equipped with specific encoding modules of high accuracy and generalization capacities. We first establish an enhanced EfficientNetV2 model for the typical chlorophyll pattern recognition tasks, with 2 attention-based modules CFG and CSF collectively employed. EfficientNetV2 bears powerful capabilities in NAS search by a compound scaling coefficient and introduces a smaller expansion ratio to compensate for memory access overhead, which jointly optimizes the accuracy, training speed, and parameter size. The network configuration is made up of convolution, mobile inverted bottleneck convolution (MBCConv), Fused-MBCConv, pooling and fully connected modules. MBCConv initially applies a 1×1 convolution to extend the dimensionality of channels, followed by a 3×3 depthwise convolution, a Squeeze-and-Excitation (SE) block, and a 1×1 convolution to reduce dimensionality. Fused-MBCConv consists of a single regular 3×3 convolution, a SE block, a 1×1 convolution.

Here the enhanced EfficientNetV2 model seamlessly integrate attention-based modules (Gao et al., 2019; Roy et al., 2018; Wang et al., 2020; Woo et al., 2018) to adaptively select the refined features of input chlorophyll distributions. First, CFG module is introduced to infer the critical channel-wise weights of chlorophyll feature maps sequentially, which exploits the inter-channel relevance, by employing average pooling and max pooling in parallel. The descriptors would forward to a shared multi-layer perceptron (MLP) to produce an addition of their critical guidance, multiplied with the initial feature map along channels. Second, CSF module is developed to incorporate salient feedback of typical chlorophyll patterns that are previously exploited insufficiently in spatial dimension complementary to channels, especially high concentration regions. The average pooling and the max pooling operations are simultaneously utilized to generate chlorophyll features of different spatial contexts across the channel, with a convolution layer applied to conclude concatenated feedback that enables to emphasize on salient features or suppress unnecessary ones. The above attention-based modules guarantee encoding the salient spatial feedback multiplied with critical channel-wise weights in EfficientNetV2, ahead of the softmax activation function, so as to potentially handle the classification problem at high accuracy.

Furthermore, DECC model is developed to explore possible typical chlorophyll patterns around eddy observations in a multi-criteria unsupervised manner. The clustering network configuration consists of one enhanced EfficientNetV2 module, convolution layer, fully connected modules, where the enhanced EfficientNetV2 mechanism is embedded to serve as an encoding function f_{θ}^{Chl} , with the similarity loss, label inference loss, mutual information loss employed during optimization. The similarity loss defines the similarity between every pair of encoded features for the typical chlorophyll patterns, to infer the possibilities that these two samples belong to the same cluster. The label inference loss is formulated to calculate the components in prediction vectors, to select highly confident cluster pseudo-labels for all the individual typical chlorophyll patterns (Wu et al., 2019). The mutual information loss elevates instance-level relationship between the deep and shallow layer representations, by considering the mutual information of the positive pairs and negative pairs from the same anchor. It guarantees a more consistent mapping, which follows joint distribution only for the same samples, otherwise, follows the marginal product distribution.

2.5. Performance Evaluation for Typical Chlorophyll Pattern Identification

2.5.1. Recognition Rate and Accuracy Index

The eddy recognition rate and accuracy index are employed here to quantify a reliable performance evaluation on typical chlorophyll patterns. The eddy recognition rate I_{rec} is defined as a ratio between the total number of verified typical chlorophyll patterns by altimeter and the total number of mesoscale eddies in the trajectory atlas with quality control:

$$I_{rec} = \frac{N_{eddies}^{Chl}}{N_{eddies}} \quad (1)$$

where N_{eddies} is the total number of all the specified mesoscale eddies in AVISO trajectory atlas for reference, of over 90% valid chlorophyll coverage. N_{eddies}^{Chl} refers to the number of eddy-induced typical patterns to be recognized within an overlapping frame of chlorophyll distribution that consistently infers toward the known eddy locations in the atlas. The accuracy index I_{ac} could be denoted as a ratio between the total number of verified typical chlorophyll patterns by altimeter and the total number of all the typical chlorophyll patterns detected as possible eddy candidates solely from chlorophyll data:

$$I_{ac} = \frac{N_{eddies}^{Chl}}{N^{Chl}} \quad (2)$$

where N^{Chl} infers the total number of estimated typical chlorophyll patterns by the recognition algorithm.

2.5.2. Concentration Ratio

Oceanic mesoscale eddies and their submesoscale fine structures are posited to exert a pronounced influence on surface chlorophyll concentration with vertical motions, which may induce vertical nutrient transports and facilitate primary productivity (Feng et al., 2022; Q. He et al., 2021). In this study, an assessment procedure has been introduced to quantify the global impact of such eddy-induced typical patterns on variations of surface chlorophyll concentration, so as to verify the possibilities in whether these mesoscale eddies and their submesoscale fine structures exert a substantial promotion on the surface chlorophyll concentration. The concentration ratio I_r of typical eddy-induced chlorophyll patterns to their background fields is defined as follows:

$$I_r = \frac{\overline{Chl}_{Typical}}{\overline{Chl}_{Background}} \quad (3)$$

where $\overline{Chl}_{Typical}$ refers to the average concentration of a specific typical chlorophyll pattern within the frame of eddy radius, and $\overline{Chl}_{Background}$ calculates the monthly average background concentration at the location of the identical frame over 20 years, by directly calculating the average chlorophyll concentration values from satellite observation for the given month in which the specific eddy occurs.

2.5.3. Wave-Number Spectrum

The spatial distribution feature of surface chlorophyll can be illustrated by the wave-number spectra, showing the contribution of perturbations at different scales and giving some clues about the dynamical origins (Burov et al., 2008; Callies & Ferrari, 2013; Denman & Abbott, 1994; Gower et al., 1980; Martin & Srokosz, 2002; Ostrovskii, 1995; Park & Chung, 1999; Smith et al., 1988; Wang et al., 2010).

A wave-number spectrum of chlorophyll concentration is first computed through a 2-D Fast Fourier Transform (FFT_2) as follows (Kleshcheva et al., 2021; Wang et al., 2020),

$$\mathcal{F}(kx, ky) = FFT_2(Chl(x, y)) \quad (4)$$

where \mathcal{F} represents the 2-D FFT of the given chlorophyll distribution $Chl(x, y)$ at the central location (x, y) , kx and ky respectively denotes the wave-number in the zonal and meridional directions. By summing up into 1 dimension, the wave-number spectrum is acquired as follows,

$$P(K) = \sum_{K=(kx^2, ky^2)^{\frac{1}{2}}} \mathcal{F}(kx, ky) \quad (5)$$

where $P(K)$ is the wave-number spectrum of chlorophyll concentration, and K represents the wave-number, and the slope of the chlorophyll concentration wave-number spectrum could be further estimated by the least squares of all the wave-number falling within the corresponding mesoscale band.

3. Results

In our simulation experiment, the developed scheme together with GlobColour Chlorophyll product has been verified by with Mesoscale Eddy Trajectory Atlas. The chlorophyll distribution time series *Chl* were involved in the global search of typical and non-typical segments from 2,954,790 eddy observations of 20 years with quality control. Three thousand positive samples and three thousand negative samples were selected unbiasedly to facilitate the training process in the enhanced EfficientNetV2 architecture, with CFG and CSF employed for a higher recognition accuracy. A total of 287,896 chlorophyll distributions were detected as eddy-induced typical patterns directly from original chlorophyll observational by the proposed model, which can be predicted as possible eddy candidates identified solely by chlorophyll observations without altimetry data involved. Further aligning with eddy locations in the trajectory atlas derived from altimetry data as references, 207,496 eddy-induced typical patterns were confirmed as real mesoscale eddies and fed into the proposed DECC model for clustering. At last, 6 potential types, including 2,372 Core, 119,469 Spiral, 25,999 Tail, 2,755 Eye, 4,961 Ring, 51,940 Loop structures, have been discovered from those typical chlorophyll distribution patterns, which will be presented with details in the following context.

3.1. Performance Evaluation for Chlorophyll Pattern Recognition

During the recognition stage, for the enhanced EfficientNetV2, the state-of-art SGD optimizer has been adopted for optimization, among which learning rate was initially set to 0.005 with the batch size of 16, by using the cross entropy with L2 regularization as the loss function. It should be noted that we examined the hyper-parameters for model selection, especially the learning rate and the batch size, to ensure their impact on the convergence of our developed model. When the batch size varied from 8 to 32 and the learning rate varied from 0.001 to 0.01, it was demonstrated from our experimental results that the selected parameters of this model exhibited quite comparable convergence with many of the state-of-the-art deep learning algorithms, such as ResNet, MobileNetV3, NF-Nets, EfficientNet B5 and the original EfficientNetV2 model, of higher accuracy and fewer Floating Point Operations (FLOPs). Great generalization ability guarantees the performances in recognizing typical surface chlorophyll patterns, so as to potentially handle the classification problem at high accuracy with low complexity. Owing to the scarcity of typical records for deep learning, we also consider data augmentation techniques to input qualified and transformed typical records to our proposed model. Thus, this method provides with one parallel pipeline that utilizes surface chlorophyll time series at a spatial high resolution to independently predict potential locations of surrounding mesoscale eddies, alongside mesoscale eddy detection and tracking algorithms previously developed for satellite altimeter. This permits us to be capable of independently identifying mesoscale eddies from the footprint of chlorophyll observations by this proposed AI framework.

Figure 2 displays a global performance evaluation of our proposed model, including the spatial distribution of recognition rate in Figure 2a and accuracy index in Figure 2b. It has been demonstrated that, during the past 20 years, 207,496 eddy observations were verified to exhibit eddy-induced typical chlorophyll patterns by our proposed scheme, accounting for approximately 22.48% of the total number of all the altimetry-based mesoscale eddies in atlas with sufficient chlorophyll coverage. This indicates that typical chlorophyll patterns emerge from locations of over 20% mesoscale eddies, with distinctly regular and consistent eddy-induced surface chlorophyll footprints. This further validates that the typical chlorophyll patterns based recognition algorithms could independently serve to identify and locate mesoscale eddies with high-resolution ocean-color satellite observations. In Figure 2a, the estimated typical chlorophyll patterns do not show to follow a uniform distribution. In the northern hemisphere, the average recognition rate of the Subtropical Counter Current (STCC), the eastern boundary of the North Pacific, the mid-latitude North Atlantic roughly reached up to 12%, 27% and 17% respectively, showing a relatively high proportion estimation of eddy-induced patterns by our proposed model, while only less than 10% of typical chlorophyll patterns have been detected around Kuroshio Extension. In the southern hemisphere, the average recognition rate in the Agulhas Current, southwestern Australia, Eastern Drake Passage Region reached around 26%, 25%, and more than 30% respectively. It has been observed that generally there are two types of regions exhibiting higher values of eddy recognition rate, the subtropical regions and the regions near continental boundaries. The former is characterized by a nutrient limit of chlorophyll growth, and the latter is featured with strong horizontal gradient of surface chlorophyll. The mesoscale eddies and their submesoscale fine structures are believed to effectively promote the enhancement of surface chlorophyll by vertical transports in subtropical regions (Guo et al., 2019; Huang & Xu, 2018; Liu & Levine, 2016), and stir the surface chlorophyll through horizontal advection in the regions near continental boundaries (Gaube et al., 2014; Wang et al., 2018), thus it

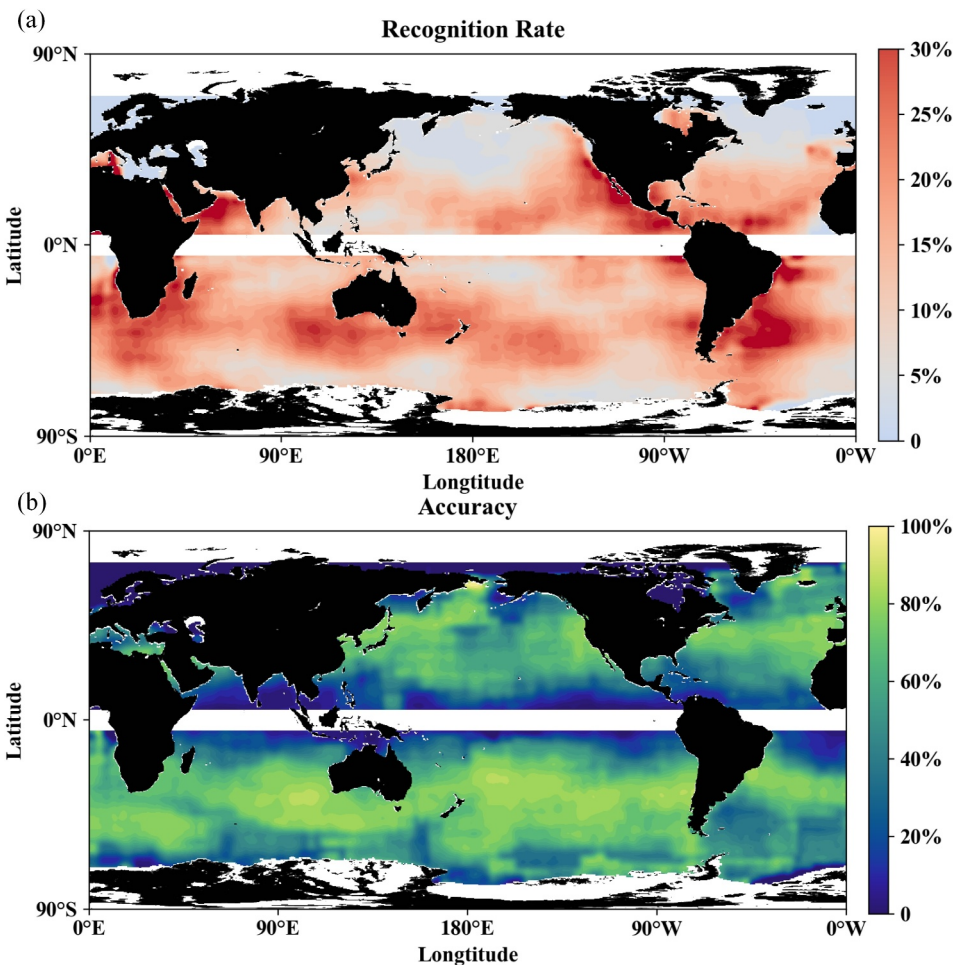


Figure 2. Performance evaluation for the typical chlorophyll pattern recognition in the global ocean via the enhanced EfficientNetV2 architecture. (a) Global spatial distribution of eddy recognition rate, reflecting the spatial distribution of the occurrence probabilities of typical chlorophyll patterns on a global scale, relative to surrounding mesoscale eddies in atlas. In other words, the recognition rate reflects how many eddies could be identified solely from the surface chlorophyll patterns related to all eddies identified by the altimetry data. (b) Global spatial distribution of accuracy index, reflecting the generalization capabilities in detecting the highly consistent typical chlorophyll patterns around individual eddy locations with high accuracy. The region of both 5° above and below the equator get removed.

tends to be more easily to leave footprints on surface chlorophyll distribution identifiable as the typical patterns in these regions. In Figure 2b, the accuracy index is distributed relatively uniform between 70% and 90% on a global view, demonstrating the consistent effectiveness and reliability of this chlorophyll based algorithm in independently identifying mesoscale eddies with potentially important biogeochemical impact. There is a notable decline of the accuracy index near the equator, partly attributed to the decreased number of the eddies in this region, which is consistent with the previous studies (Chelton et al., 2011; Zhao et al., 2021). To be noted, here we establish a set of strict learning criteria in modeling AI framework which automatically identifies the most typical chlorophyll patterns. Although over 20% mesoscale eddy observations exhibit identifiable typical chlorophyll patterns, the current recognition rate is believed to serve as an underestimated lower limit. The actual number of eddies with potentially qualified chlorophyll footprints are expected to far exceed 20%, as a considerable number of less typical chlorophyll patterns, either below high confidence levels during inference, or of ambiguous distribution characteristics, have been categorized as non-typical eddy-induced chlorophyll patterns, as is shown in Figure S1 of Supporting Information S1. By employing such rigorous criteria, we ensure that the typical chlorophyll patterns in eddy-associated chlorophyll analysis possessed high reliability and accuracy, although this might have led to the omission of some other potentially qualified chlorophyll footprints. Further analysis in the statistics of 20-

year regional recognition rate and accuracy index verified consistently good performances in modeling the regional generalization of our proposed scheme, regardless the seasons.

The spatial and temporal mapping of the global chlorophyll concentration ratio I_c is shown in Figure 3, where the average chlorophyll concentration ratio at each grid is computed as the average values within a surrounding $5^\circ \times 5^\circ$ window with global 20-year observations. Overall, those mesoscale eddies that induce typical chlorophyll patterns tend to increase the surface chlorophyll concentration globally, especially enhancing by approximately 10%–30% in subtropical regions and multiple coastal regions, even maximally reaching up to 50% in some specific regions. On a global scale, Figures 3a and 3b delineate 20-year spatial distribution of the average chlorophyll concentration ratio for the spring-summer period (March, April, May, June, July, August) and the autumn-winter period (September, October, November, December, January) of all the individual years, respectively. Most regions exhibit an increasing tendency of the chlorophyll concentration by typical eddy-induced patterns, compared to the corresponding background value. During the spring-summer period of each year, the larger chlorophyll concentration ratio emerges in the northern hemisphere, especially regions around STCC, the eastern boundary of the North Pacific, the Gulf Stream, in comparison with that of the southern hemisphere. On the contrary, during the autumn-winter period of each year, the enhancement in the southern hemisphere exceeds most of the northern hemisphere, and in particular, the east and west sides of Australia, the east side of the Drake Passage, reveal more evidently enhanced chlorophyll concentration for typical eddy-induced patterns. In order to give a more clear picture of this seasonal variation, Figure 3c illustrates the monthly variation in the chlorophyll concentration ratio of both the southern and northern hemispheres, which indicates a monthly reversed growth trends in these two hemispheres. While for each hemisphere, the concentration ratio all tends to gradually start increases in their individual springs, with a noticeable trend to peak values in transition to summers, and then appears a moderately decrease as summers turn to autumns, and reaches the valley values in their individual winters. It is also notable, the minimum concentration values of the two curves are still larger than 114%, which means the typical chlorophyll patterns in general promote the increase of the surface chlorophyll concentration globally. On average, the overall chlorophyll concentration ratio of all the existing typical patterns reaches to 121% globally. Additionally, it has been demonstrated from our further correlation analysis in strain rate, eddy amplitude, SST gradient that stronger eddies favor higher chlorophyll concentration of the typical patterns, regardless their polarity, as is shown in Figure S2 of Supporting Information S1. As an indicator for the frontogenesis processes, higher strain rate results in higher chlorophyll concentration of the typical patterns. As an indicator for the mixed layer instability processes, higher SST gradient leads to higher chlorophyll concentration of the typical patterns. This indicates a general relationship between the typical chlorophyll patterns and the frontal processes on mesoscale eddies.

3.2. Clustering Analysis of Typical Chlorophyll Patterns

During the clustering stage, our proposed DECC model employed the state-of-the-art root mean square propagation (RMSprop) optimizer, with the decay coefficient α 5, and the learning rate was initially set to 0.0001 with the batch size of 64 after model selection. Starting from an adequate number of clusters, the clustering earned activation for winner and assigned penalty for their rivals, with the help of membership, so that the effective number of clusters could be preliminarily determined during learning. In this way, six categories of typical chlorophyll patterns with distinct geometrical characteristics, have been grouped. Figure 4 shows example chlorophyll distribution images at different geometries, which have been assigned into separate clusters of Core, Spiral, Tail, Ring, Loop, Eye, with different geometrical characteristics, by our DECC algorithm. It can be observed that the Core type reflects in the enhancement of chlorophyll concentration around the eddy center, which is commonly caused by high-chlorophyll water mass trapped at eddy center and transported by the corresponding eddies, or by the Ekman upwelling at eddy center induced by wind-current interaction (Gaube et al., 2013, 2014, 2015; Q. He et al., 2016; McGillicuddy, 2016). Spiral type presents a spiral-shaped chlorophyll enhancement. These spiral chlorophyll bands have also been identified and revealed as footprints of vortex Rossby Waves by the former research (Zhang & Qiu, 2020), which only found the spatial structure with single spiral arm. As is shown in the second case in Figure 4b, the DECC model here not only successfully identified the single-arm spiral band, but also revealed the spiral structures with multiple arms, which demonstrates the advantages of our AI approach. Tail type is a composite of Core type and Spiral type, showing the enhanced chlorophyll concentration in the eddy center region, accompanied with a spiral-shaped tail. The Ring type exhibits

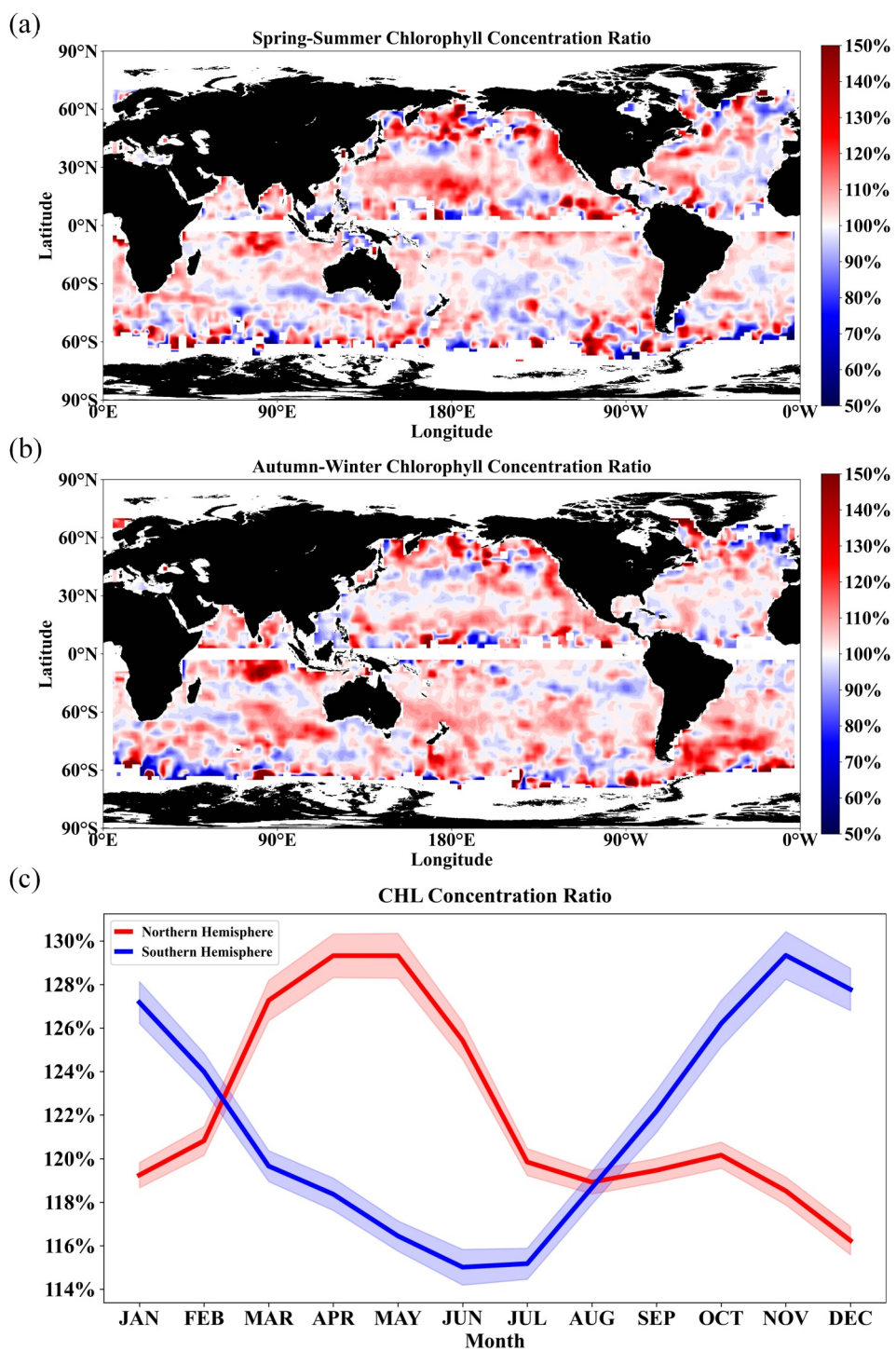


Figure 3. 20-year global chlorophyll concentration ratio mapping. (a) Spatial distribution of average chlorophyll concentration ratio for the spring-summer period of individual years. (b) Spatial distribution of average chlorophyll concentration ratio for the autumn-winter period of individual years. (c) Temporal distribution of the chlorophyll concentration ratio, with monthly variation of the northern hemisphere in red and southern hemisphere in blue. The monthly average chlorophyll concentration ratio for each hemisphere is calculated as the mean monthly ratio values from 1998 to 2017. The regions of both 5° above and below the equator are removed.

the enhanced chlorophyll concentration at the edges of oceanic eddies in a circular pattern, which may emerge from combination effect of horizontal advection and wind-current interaction (McGillicuddy, 2016; Xu et al., 2019). The Loop type displays a side-passed curve structure around the eddies, which may induce the

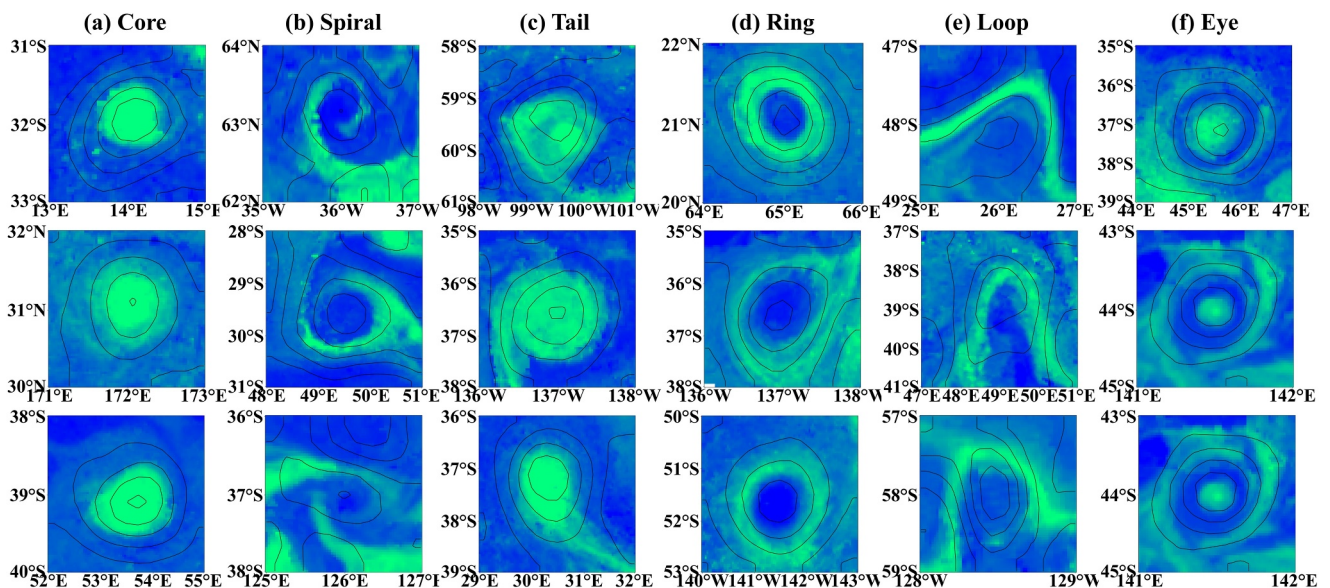


Figure 4. Example typical chlorophyll patterns of six categories by our clustering algorithm. (a) Core; (b) Spiral; (c) Tail; (d) Ring; (e) Loop; (f) Eye. The green shade represents the chlorophyll concentration, and black solid lines denote SLA contours.

enhancement of surface chlorophyll by frontal upwelling and advection of mesoscale meandering current, as is shown in Figure S4 of Supporting Information S1 (Chelton et al., 2011). Finally, the Eye type presents a combination of Core/Ring or Core/Loop, with high chlorophyll concentration covering both the eddy center and the edges of the eddies. Generally speaking, among six types of typical chlorophyll patterns, the number of identifiable cyclonic eddies is more than that of anticyclonic eddies in most cases, while the Loop type exhibits an opposite trend in quantity, as is shown in Figure S3 of Supporting Information S1. In our study, regardless of the direction of high chlorophyll trail, the Spiral and Tail types of chlorophyll distribution could be automatically grouped into the same types by our developed scheme, which exhibits high robustness and generalization ability. To be noted, besides a great many of positive chlorophyll anomalies with higher chlorophyll concentration in the eddy centers, like the Core type, the Tail type, etc., some depressed chlorophyll patterns are also observed with lower chlorophyll concentration in the eddy centers, which is consistent to the previous studies (Chelton et al., 2011; Gaube et al., 2013, 2014; McGillicuddy, 2016), and most of them have been automatically identified as Ring type by our clustering algorithm, as is shown in Figure S5 of Supporting Information S1. This clustering scheme guarantees to be applicable to the potential new clusters that have never been seen too, when feeding with unknown types of chlorophyll distribution samples newly observed.

The total number of the observed typical eddy-induced patterns from each category, determined by our clustering algorithm, is further calculated and globally projected at each grid, as is shown in Figure 5. It could be discovered that although the number of the typical patterns in each category follows a relatively identical spatial distribution worldwide, that is, larger values highly consistently congregate to a number of specific locations, including the eastern boundary of the North Pacific, Gulf Stream, Agulhas Current, eastern and western side of Australia, Peru upwelling and the eastern side of the Drake Passage, for each grid, the proportions between the total number of typical patterns from each cluster and all clusters exhibits significantly diverse. In statistics, the type of Core pattern only accounts for 1% probability of occurrence in all kinds of typical chlorophyll patterns, in particular widely distributed to the west side of Hawaii, besides the above commonly distributed locations. The Spiral type constitutes roughly 59% of all the globally distributed typical chlorophyll patterns, which is of the highest occurrence probability in the six categories. To be concrete, the Spiral type demonstrates more prevalent spatial distribution from STCC to Hawaii, from the middle to the high latitudes of the North Atlantic, in the northern hemisphere. Meanwhile, this type distributes extensively from the east and west side of Australia to Cape of Good Hope, with a concentration in the Agulhas Current region, showing a strong continuous band-like spatial distribution, extensible along the middle latitudes in the southern hemisphere. In aid of our clustering technique, the chlorophyll patterns of the Spiral type have been automatically identified with a highly efficient calculation. The

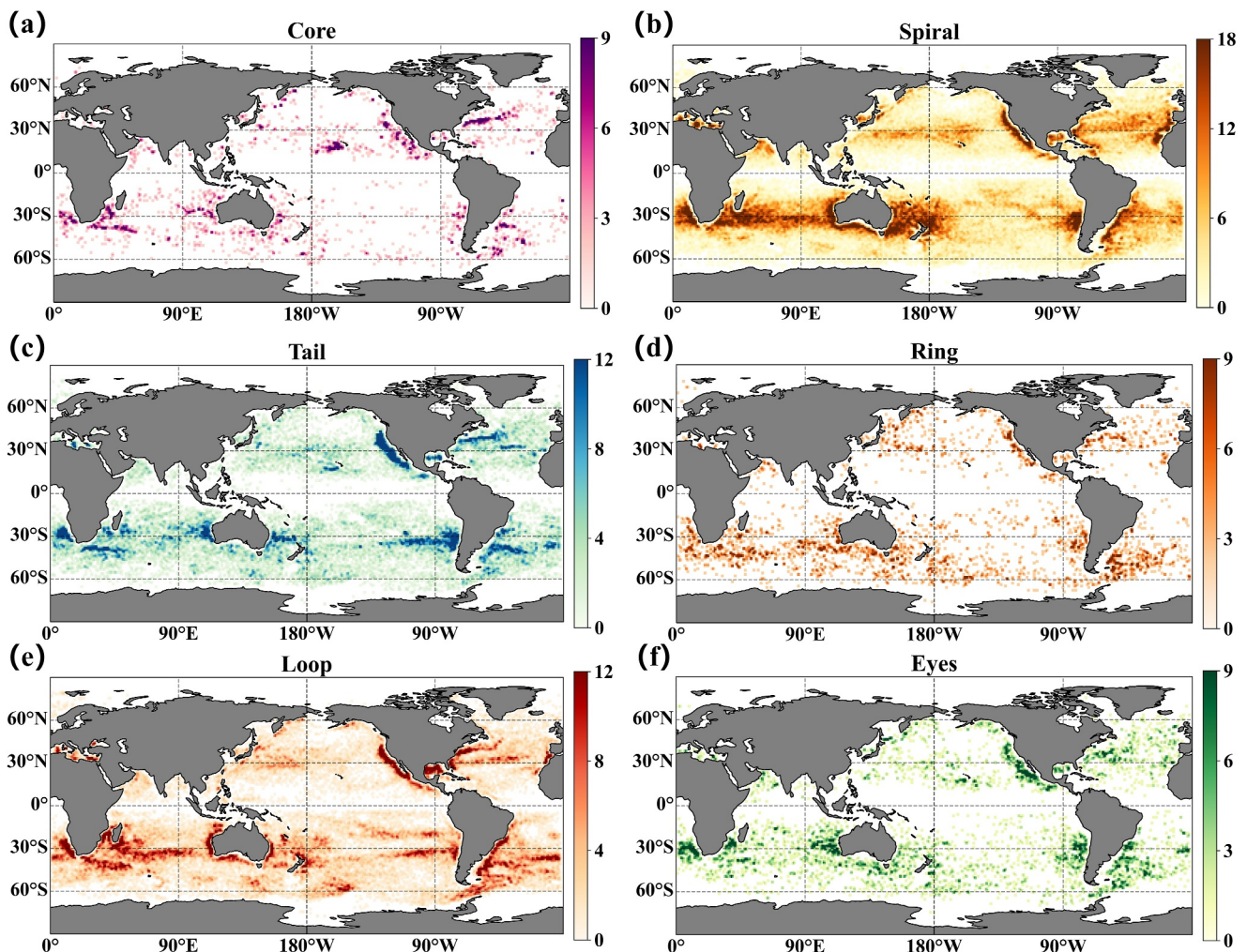


Figure 5. The spatial distribution of 6 typical chlorophyll patterns. (a) Core; (b) Spiral; (c) Tail; (d) Ring; (e) Loop; (f) Eye. At each grid, the color intensity in the global spatial distribution indicates the occurrence frequency of typical chlorophyll patterns in each category, calculated within a $1^\circ \times 1^\circ$ grid. The darker the color intensity is, the greater number of typical patterns is observed for each category.

resulting spatial distribution of the Spiral type exhibits a highly consistent estimation to the previous work with a specifically designed quantitative criteria to retrieve spiral-band shaped chlorophyll patterns around mesoscale eddies (Zhang & Qiu, 2020), proving its effectiveness and versatility in this unsupervised learning. The Tail type, which could be seen as a composite between the Core and Spiral types, occupied about 12% of all the typical chlorophyll patterns, with a widespread spatial distribution at locations where both the Core and Spiral types are primarily present. The Ring type also accounts for approximately 1% of all the typical chlorophyll patterns, with a relatively even global distribution. The Loop type, distributed differently from the Spiral type in the southern hemisphere, with several short but disconnected bands, accounts around 24% of the typical chlorophyll patterns by the clustering algorithm. The Eye type, characterized by a combination of the Core and Loop or Ring types, happens to represent around 3% of the typical chlorophyll patterns, distributed comparable to the Core type, with a significant enhancement in the ocean regions dominated by the Loop and Ring types. Although some of the Ring type eddies exhibit negative chlorophyll anomalies at eddy center (Chelton et al., 2011; Gaube et al., 2013, 2014; McGillicuddy, 2016; Xu et al., 2019), in total, they only exert a relatively minor influence on the surface chlorophyll concentration globally, compared to other types of typical chlorophyll patterns, so the mesoscale eddies with typical eddy-induced patterns tend to collectively regulate a global increase of the surface chlorophyll concentration.

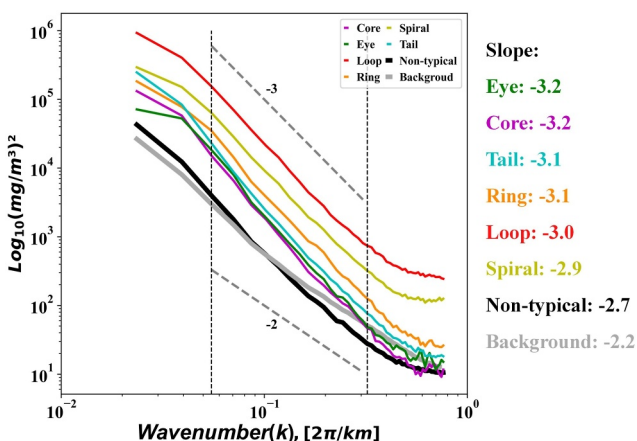


Figure 6. Wave-number spectrum curves for the global chlorophyll concentration, with the type of Eye, Core, Tail, Ring, Loop, Spiral, respectively in purple, green, red, orange, yellow, blue, the non-typical distribution in black, and the non-eddy background in gray. The gray dashed lines serve as the prompt lines of the slopes -2 and -3 .

tribution projects the flattest curve of the slope -2.2 . The around-eddy but non-typical spectrum bears a relatively steeper slope of -2.7 , implying that even for those mesoscale eddies without typical chlorophyll patterns, their advection, propagation and evolution still bring the spectrum visible impact on variations of chlorophyll concentration to some extent. As a whole, eddy-induced typical patterns within the mesoscale band exhibit a significantly steeper slope near -3 , compared to the above two spectrum, with the spectrum slope of the Spiral, Loop, Ring, Tail, Core, Eye types -2.9 , -3.0 , -3.1 , -3.1 , -3.2 and -3.2 respectively. These spectral slopes range from several kilometers to about hundred kilometers, where the mesoscale eddies and their fine structures have considerable impact on the surface chlorophyll distributions, and will further induce diverse wave-number spectral slopes of chlorophyll as tracers (Horwood, 1978; McWilliams, 2010, 2016; Smith et al., 1988).

In general, the occurrence of typical chlorophyll patterns inevitably corresponds to one or more specific dynamical processes, such as horizontal advection, trapping, and Ekman upwelling/downwelling, etc (Chelton et al., 2011; Chen et al., 2007; Frenger et al., 2018; Gaube et al., 2014, 2015; Q. He et al., 2016; Klein & Lapeyre, 2009; Mahadevan, 2016; McGillicuddy, 2016; McGillicuddy et al., 2007; Siegel et al., 1999; Xu et al., 2019). However, it is still of challenging to fully explain the occurrence of these typical patterns by mesoscale advection or pure biogeochemical processes, and some specific mesoscale and submesoscale dynamics might be involved. The chlorophyll wave-number spectrum performs as an indicator to quantitatively estimate the degree of spatial heterogeneity of the surface chlorophyll distribution, and provides more insight into the underlying mesoscale and submesoscale dynamics, which may refer to different kinds of ageostrophic instabilities, and resultant horizontal or vertical advects by the mesoscale and submesoscale flow field, and other possible processes (Abraham & Bowen, 2002; Bracco et al., 2009; Garrett & Munk, 1975; Weichman & Glazman, 2002; Zhang & Qiu, 2020). One of the typical patterns, the spiral chlorophyll bands, can be theoretically explained as the biogeochemical footprints induced by vortex Rossby waves (Zhang & Qiu, 2020). Other fine structures of mesoscale eddies, for example, Chlorophyll Rings (CRs), have been identified to be driven by potential generation mechanisms, like horizontal advection and wind-current interaction (McGillicuddy, 2016; Xu et al., 2019). The monopole pattern of surface chlorophyll can also emerge from eddy trapping, Ekman pumping by wind-current interaction, and vertical displacement of isopycnal surfaces by mesoscale eddy evolution (Gaube et al., 2013, 2014, 2015; Q. He et al., 2016). The loop structure of surface chlorophyll distribution may emerge from the enhancement of surface chlorophyll by the frontal upwelling and advection of mesoscale meandering current (Chelton et al., 2011). In our study, it has been further shown that these typical chlorophyll patterns are not solely passive tracers but also active tracers that are potentially determined by mesoscale eddies and submesoscale dynamics, while the dynamical processes underlying the remaining typical chlorophyll patterns are still calling for future research, which is well beyond the scope of this paper.

3.3. Tracer Wave-Number Spectrum Calculation

The spatial wave-number spectrum is generally computed for three types of chlorophyll distribution, that is, the verified eddy-induced typical patterns, the around-eddy but non-typical distribution, and the non-eddy background distribution. The first two items all refer to chlorophyll distribution of the known eddy locations in the altimetry derived atlas. The former involves all the 207,496 eddy observations that have been consistently confirmed by our recognition model, while the latter corresponds to non-typical chlorophyll distribution around the rest of the known eddy observations in the atlas. Both these two items denote the search region of 2.5 times eddy radius for the chlorophyll concentration values by aligning to eddy center coordinates. The last item is retrieved from the global chlorophyll time series by removing all the eddy-influenced distribution regions. With the help of the clustering, the eddy-induced typical patterns would be further subdivided into six categories for individual wave-number spectrum calculations.

The wave-number spectrum of chlorophyll concentration for six eddy-induced typical patterns, for the around-eddy but non-typical distribution, and for the non-eddy background distribution, are sketched in Figure 6, respectively. Among them, the spectrum of the non-eddy background dis-

4. Conclusions and Discussion

In this study, different types of typical chlorophyll patterns were identified around mesoscale eddies by a deep learning based model, for over 20 years of satellite remote sensing chlorophyll data. A total of 207,496 eddy observations were verified to exhibit eddy-induced typical chlorophyll patterns. It is demonstrated that the typical eddy-induced patterns tended to increase the surface chlorophyll concentration within the corresponding eddies and exhibit significant seasonal variation in both hemispheres, especially enhancing surface chlorophyll by 30% in nutrient-restricted subtropical regions compared with the background values; The AI framework automatically explored 6 specific types of the typical chlorophyll patterns, namely Core, Spiral, Tail, Eye, Loop, and Ring, in the context of the generally comparable geometric characteristics that are potentially reflected by their underlined oceanic dynamics. Further spatial-spectral analysis found that the typical patterns on eddies exhibited a much steeper wave-number spectral slope roughly -3 , compared to the non-typical distributions around eddies and the non-eddy background distribution (about -2.7 – -2.2). This implies that occurrence of different typical chlorophyll patterns may not be explained solely by mesoscale advection or pure biogeochemical processes, and some specific mesoscale and submesoscale dynamics can be involved.

Most of the recent studies primarily focus on the formation mechanism of submesoscale processes by different kinds of instabilities, but what spatial structures emerge from these instability processes has not been provided with comprehensive answers, not to mention the underlying mesoscale to submesoscale dynamics. Here, by using an artificial intelligence algorithm to identify and classify six types of typical chlorophyll patterns of mesoscale eddies, we hope to shine some light along this line and promote further detailed dynamical studies. This is possible and there was an already successful example that the submesoscale spiral chlorophyll bands can be explained by the vortex Rossby waves (Zhang & Qiu, 2020). Understanding how these patterns evolve over time with mesoscale eddies on a global scale and the underlying physical mechanisms is an exploratory question for future research.

Since the current study primarily focuses on developing AI techniques that could automatically identify typical surface chlorophyll patterns of mesoscale eddies, it remains unknown about the possible patterns of vertical chlorophyll distributions induced by mesoscale eddies from a 3D perspective, which is of importance to be taken into in-depth account in the future research. Although remote sensing water color mapping provide a huge number of near-surface chlorophyll observations, the direct and detailed observations on deeper ocean layers are still needed, which may depend on in-situ platforms like Bio-Argo. It is to be hoped that the rapid development of deep learning capabilities could provide opportunities to help reconstruct the distribution and variation on 3D fields of ocean chlorophyll concentration at diverse depth in the near future.

Meanwhile, this study only makes use of the surface chlorophyll data to fulfill the identification tasks for mesoscale eddies and their submesoscale fine structures. Since the other remote sensing observations, for example, SST, also leave their abundant footprints from mesoscale eddies, as a future perspective, it will be of a great interest to provide additional predictors, for instance, including input from satellite products of sea surface temperature, or other ocean bio-chemical and physical variables, together with surface chlorophyll distribution, to the modeling of the deep learning framework. Further work could also extend this approach to comprehensively improve our understanding in the characteristics of mesoscale eddies and their submesoscale fine structures, allowing to develop a more efficient and accurate identification scheme.

Moreover, most of the current studies mainly concentrate on the spatial distribution of ocean chlorophyll concentration, while it might be lack of much consideration in evaluating the temporal variations of chlorophyll distribution. The temporal evolution of surface chlorophyll associated with mesoscale eddies over entire eddy lifespan is complicated (Huang et al., 2017). In our study, we have found that different types of typical chlorophyll patterns might transform to each other in the process of eddy evolution. In the future, we will further extend our proposed identification strategies to systematically investigate the temporal variations between typical chlorophyll patterns around mesoscale eddies and their submesoscale fine structures, in addition to the spatial distribution.

Mesoscale eddies and submesoscale fine structures are believed to be able to produce significant vertical motion, making a considerable contribution to the vertical flux of nutrients and primary productivity (Falkowski et al., 1991; Field et al., 1998). This study highlights typical chlorophyll patterns of multiple sub- and mesoscale fine structures that significantly enhance the surface chlorophyll concentration, which might be partially caused

by biogeochemical footprints of the vertical motions from mesoscale eddies and their submesoscale processes. Quantitative estimations are given about how much the concentration of typical chlorophyll patterns enhance with their spatial distribution, as well as the wave-number spectra of different types of typical chlorophyll patterns. Our results may provide help to establish parameterizations of the effect of submesoscale processes or an observational baseline to verify some high-resolution physical-biogeochemical coupled oceanic numerical models, and improve the model simulations of primary productivity and carbon fixation capacity, in the context of global warming.

Conflict of Interest

The authors declare no conflicts of interest relevant to this study.

Data Availability Statement

The mesoscale eddy trajectory atlas product can be accessed from the AVISO website (<https://www.aviso.altimetry.fr/en/data/products/value-added-products/global-mesoscale-eddy-trajectory-product.html>). The chlorophyll product in our study, is available from European Space Agency (ESA) GlobColour Project (<https://globcolour.info>). The implementation of AI algorithms in the typical surface chlorophyll pattern identification uses open source software python 3.8 and python packages including matplotlib 3.8.3 (<https://pypi.org/project/matplotlib/>), pytorch 1.11.0 (<https://pytorch.org/>).

Acknowledgments

This research was supported by the National Natural Science Foundation of P. R. China under Grants 42376191, 42288101 and 42022041, National Key R&D Program under Grant 2019YFC1408304, National Key R&D Program under Grant 2016YFC0301400, National High-Tech R&D 863 Program under Grant 2014AA093410. The authors want to thank “Qingdao AI Computing Center” and “Eco-Innovation Center” for providing inclusive computing power and technical support of MindSpore during the completion of this paper.

References

- Abraham, E. R., & Bowen, M. M. (2002). Chaotic stirring by a mesoscale surface-ocean flow. *Chaos: An Interdisciplinary Journal of Nonlinear Science*, 12(2), 373–381. <https://doi.org/10.1063/1.1481615>
- Bachman, S. D., Fox-Kemper, B., Taylor, J. R., & Thomas, L. N. (2017). Parameterization of frontal symmetric instabilities. I: Theory for resolved fronts. *Ocean Modelling*, 109, 72–95. <https://doi.org/10.1016/j.ocemod.2016.12.003>
- Bachman, S. D., & Taylor, J. R. (2014). Modelling of partially-resolved oceanic symmetric instability. *Ocean Modelling*, 82, 15–27. <https://doi.org/10.1016/j.ocemod.2014.07.006>
- Bennetts, D. A., & Hoskins, B. J. (1979). Conditional symmetric instability—a possible explanation for frontal rain bands. *Quarterly Journal of the Royal Meteorological Society*, 105(446), 945–962. <https://doi.org/10.1002/qj.49710544615>
- Boccaletti, G., Ferrari, R., & Fox-Kemper, B. (2007). Mixed layer instabilities and rest ratification. *Journal of Physical Oceanography*, 37(9), 2228–2250. <https://doi.org/10.1175/JPO3101.1>
- Bracco, A., Clayton, S., & Pasquero, C. (2009). Horizontal advection, diffusion, and plankton spectra at the sea surface. *Journal of Geophysical Research*, 114(C2). <https://doi.org/10.1029/2007JC004671>
- Buckingham, C. E., Khaleel, Z., Lazar, A., Martin, A. P., Allen, J. T., Garabato, A. C., et al. (2017). Testing Munk's hypothesis for submesoscale eddy generation using observations in the North Atlantic. *Journal of Geophysical Research*, 122(8), 6725–6745. <https://doi.org/10.1002/2017JC012910>
- Burov, D. V., Permyakov, M. S., & Tarkhova, T. I. (2008). Osobennosti prostranstvennoi izmenchivosti polei gidrologicheskikh i bioopticheskikh elementov v razlichnykh raionakh Mirovogo okeana (Features of the spatial variability of hydrological and biological fields of optical elements in different areas of the oceans). *Sovremennye problemy distantsionnogo zondirovaniya Zemli iz kosmosa*, 2(5), 62–68.
- Callies, J., & Ferrari, R. (2013). Interpreting energy and tracer spectra of upper-ocean turbulence in the submesoscale range (1–200 km). *Journal of Physical Oceanography*, 43(11), 2456–2474. <https://doi.org/10.1175/JPO-D-13-063.1>
- Capet, X., McWilliams, J. C., Molemaker, M. J., & Shchepetkin, A. J. (2008). Mesoscale to submesoscale transition in the California current system. Part I: Flow structure, eddy flux, and observational tests. *Journal of Physical Oceanography*, 38(1), 29–43. <https://doi.org/10.1175/2007JPO3671.1>
- Chelton, D. B., Gaube, P., Schlax, M. G., Early, J. J., & Samelson, R. M. (2011). The influence of nonlinear mesoscale eddies on near-surface oceanic chlorophyll. *Science*, 334(6054), 328–332. <https://doi.org/10.1126/science.1208897>
- Chen, X., Chen, G., Ge, L., Huang, B., & Cao, C. (2021). Global oceanic eddy identification: A deep learning method from Argo profiles and altimetry data. *Frontiers in Marine Science*, 8, 646926. <https://doi.org/10.3389/fmars.2021.646926>
- Chen, Y. L. L., Chen, H. Y., Lin, I. I., Lee, M. A., & Chang, J. (2007). Effects of cold eddy on phytoplankton production and assemblages in Luzon Strait bordering the South China Sea. *Journal of Oceanography*, 63(4), 671–683. <https://doi.org/10.1007/s10872-007-0059-9>
- Colas, F., Capet, X., McWilliams, J. C., & Li, Z. (2013). Mesoscale eddy buoyancy flux and eddy-induced circulation in eastern-boundary currents. *Journal of Physical Oceanography*, 43(6), 1073–1095. <https://doi.org/10.1175/JPO-D-11-0241.1>
- Denman, K. L., & Abbott, M. R. (1994). Time scales of pattern evolution from cross-spectrum analysis of advanced very high resolution radiometer and coastal zone color scanner imagery. *Journal of Geophysical Research*, 99(C4), 7433–7442. <https://doi.org/10.1029/93JC02149>
- Du, Y., Dong, X., Jiang, X., Zhang, Y., Zhu, D., Sun, Q., et al. (2021). Ocean surface current multiscale observation mission (OSCOM): Simultaneous measurement of ocean surface current, vector wind, and temperature. *Progress in Oceanography*, 193, 102531. <https://doi.org/10.1016/j.pocean.2021.102531>
- Elistratov, S. A., Vatutin, K. A., Sibgatullin, I. Y. N., Yermayuk, E. V. E., & Mikhaylov, E. A. (2020). Numerical simulation of internal waves and effects of accumulation of kinetic energy in large aspect ratio domains. *Proceedings of the Institute for System Programming of the RAS*, 32(6), 200–212. [https://doi.org/10.15514/ISPRAS-2020-32\(6\)-15](https://doi.org/10.15514/ISPRAS-2020-32(6)-15)
- Falkowski, P. G., Zieman, D., Kolber, Z., & Bienfang, P. K. (1991). Role of eddy pumping in enhancing primary production in the ocean. *Nature*, 352(6330), 55–58. <https://doi.org/10.1038/352055a0>
- Feng, N. A. N., Fei, Y. U., Anqi, X. U., & Yanan, D. I. N. G. (2022). Progress and prospect of subsurface-intensified eddies in the northwestern Pacific Ocean. *Advances in Earth Science*, 37(11), 1115. <https://doi.org/10.11867/j.issn.1001-8166.2022.061>

- Ferrari, R., & Wunsch, C. (2009). Ocean circulation kinetic energy-Reservoirs, sources, and sinks. *Annual Review of Fluid Mechanics*, 41(1), 253–282. <https://doi.org/10.1146/annurev.fluid.40.111406.102139>
- Field, C. B., Behrenfeld, M. J., Randerson, J. T., & Falkowski, P. (1998). Primary production of the biosphere: Integrating terrestrial and oceanic components. *Science*, 281(5374), 237–240. <https://doi.org/10.1126/science.281.5374.237>
- Fox-Kemper, B., Ferrari, R., & Hallberg, R. W. (2008). Parameterization of mixed layer eddies. I. Theory and diagnosis. *Journal of Physical Oceanography*, 38(6), 1145–1165. <https://doi.org/10.1175/2007JPO3792.1>
- Frenger, I., Münnich, M., & Gruber, N. (2018). Imprint of Southern Ocean mesoscale eddies on chlorophyll. *Biogeosciences*, 15(15), 4781–4798. <https://doi.org/10.5194/bg-15-4781-2018>
- Gao, Z., Xie, J., Wang, Q., & Li, P. (2019). Global second-order pooling convolutional networks. In *Proceedings of the IEEE/CVF Conference on Computer Vision and Pattern Recognition* (pp. 3024–3033). <https://doi.org/10.48550/arXiv.1811.12006>
- Garrett, C., & Munk, W. (1975). Space-time scales of internal waves: A progress report. *Journal of Geophysical Research*, 80(3), 291–297. <https://doi.org/10.1029/JC080i003p00291>
- Gaube, P., Chelton, D. B., Samelson, R. M., Schlax, M. G., & O'Neill, L. W. (2015). Satellite observations of mesoscale eddy-induced Ekman pumping. *Journal of Physical Oceanography*, 45(1), 104–132. <https://doi.org/10.1175/JPO-D-14-0032.1>
- Gaube, P., Chelton, D. B., Strutton, P. G., & Behrenfeld, M. J. (2013). Satellite observations of chlorophyll, phytoplankton biomass, and Ekman pumping in nonlinear mesoscale eddies. *Journal of Geophysical Research: Oceans*, 118(12), 6349–6370. <https://doi.org/10.1002/2013JC009027>
- Gaube, P., McGillicuddy, D. J. Jr., Chelton, D. B., Behrenfeld, M. J., & Strutton, P. G. (2014). Regional variations in the influence of mesoscale eddies on near-surface chlorophyll. *Journal of Geophysical Research: Oceans*, 119(12), 8195–8220. <https://doi.org/10.1002/2014JC010111>
- Goodfellow, I. J., Pouget-Abadie, J., Mirza, M., Xu, B., Warde-Farley, D., Ozair, S., et al. (2014). Generative adversarial nets. *Advances in Neural Information Processing Systems*, 27. <https://doi.org/10.5555/296903.2969125>
- Gower, J. F. R., Denman, K. L., & Holter, R. J. (1980). Phytoplankton patchiness indicates the fluctuation spectrum of mesoscale oceanic structure. *Nature*, 288(5787), 157–159. <https://doi.org/10.1038/288157a0>
- Guo, M., Xiu, P., Chai, F., & Xue, H. (2019). Mesoscale and submesoscale contributions to high sea surface chlorophyll in subtropical gyres. *Geophysical Research Letters*, 46(22), 13217–13226. <https://doi.org/10.1029/2019GL085278>
- Haine, T. W., & Marshall, J. (1998). Gravitational, symmetric, and baroclinic instability of the ocean mixed layer. *Journal of Physical Oceanography*, 28(4), 634–658. [https://doi.org/10.1175/1520-0485\(1998\)028<0634:GSABIO>2.0.CO;2](https://doi.org/10.1175/1520-0485(1998)028<0634:GSABIO>2.0.CO;2)
- Ham, Y. G., Kim, J. H., & Luo, J. J. (2019). Deep learning for multi-year ENSO forecasts. *Nature*, 573(7775), 568–572. <https://doi.org/10.1038/s41586-019-1559-7>
- He, K., Zhang, X., Ren, S., & Sun, J. (2016). Deep residual learning for image recognition. In *Proceedings of the IEEE Conference on Computer Vision and Pattern Recognition* (pp. 770–778). <https://doi.org/10.48550/arXiv.1512.03385>
- He, Q., Mo, D., Zhan, W., Cai, S., Tang, S., Zha, G., & Zhan, H. (2024). Thermal imprints of mesoscale eddies in the global ocean. *Journal of Physical Oceanography*, 54(9), 1991–2009. <https://doi.org/10.1175/JPO-D-23-0226.1>
- He, Q., Zhan, H., Cai, S., & Zha, G. (2016). On the asymmetry of eddy-induced surface chlorophyll anomalies in the southeastern Pacific: The role of eddy-Ekman pumping. *Progress in Oceanography*, 141, 202–211. <https://doi.org/10.1016/j.pocean.2015.12.012>
- He, Q., Zhan, H., Cai, S., & Zhan, W. (2021). Eddy-induced near-surface chlorophyll anomalies in the subtropical Gyres: Biomass or Physiology? *Geophysical Research Letters*, 48(7), e2020GL091975. <https://doi.org/10.1029/2020GL091975>
- Hinton, G. E., Osindero, S., & Teh, Y. W. (2006). A fast learning algorithm for deep belief nets. *Neural Computation*, 18(7), 1527–1554. <https://doi.org/10.1162/neco.2006.18.7.1527>
- Horwood, J. W. (1978). Observations on spatial heterogeneity of surface chlorophyll in one and two dimensions. *Journal of the Marine Biological Association of the United Kingdom*, 58(2), 487–502. <https://doi.org/10.1017/S0025315400028149>
- Hoskins, B. J. (1982). The mathematical theory of frontogenesis. *Annual Review of Fluid Mechanics*, 82(1), 131–151. <https://doi.org/10.1146/annurev.fl.14.010182.001023>
- Hoskins, B. J., & Bretherton, F. P. (1972). Atmospheric frontogenesis models: Mathematical formulation and solution. *Journal of the Atmospheric Sciences*, 29(1), 11–37. [https://doi.org/10.1175/1520-0469\(1972\)029<0011:afmmfa>2.0.co;2](https://doi.org/10.1175/1520-0469(1972)029<0011:afmmfa>2.0.co;2)
- Howard, A. G., Zhu, M., Chen, B., Kalenichenko, D., Wang, W., Weyand, T., et al. (2017). Mobilenets: Efficient convolutional neural networks for mobile vision applications. *arXiv preprint arXiv:1704.04861*. <https://doi.org/10.48550/arXiv.1704.04861>
- Hu, S., Lu, X., Li, S., Wang, F., Guan, C., Hu, D., et al. (2021). Multi-decadal trends in the tropical Pacific western boundary currents retrieved from historical hydrological observations. *Science China Earth Sciences*, 64(4), 600–610. <https://doi.org/10.1007/s11430-020-9703-4>
- Huang, G., Liu, Z., Van Der Maaten, L., & Weinberger, K. Q. (2017). Densely connected convolutional networks. In *Proceedings of the IEEE Conference on Computer Vision and Pattern Recognition* (pp. 4700–4708). <https://doi.org/10.1109/CVPR.2017.243>
- Huang, J., & Xu, F. (2018). Observational evidence of subsurface chlorophyll response to mesoscale eddies in the North Pacific. *Geophysical Research Letters*, 45(16), 8462–8470. <https://doi.org/10.1029/2018GL078408>
- Jing, Z., Fox-Kemper, B., Cao, H., Zheng, R., & Du, Y. (2021). Submesoscale fronts and their dynamical processes associated with symmetric instability in the northwest Pacific subtropical ocean. *Journal of Physical Oceanography*, 51(1), 83–100. <https://doi.org/10.1175/JPO-D-20-0076.1>
- Kalvankar, S., Pandit, H., & Parwate, P. (2020). Galaxy morphology classification using efficientnet architectures. *arxiv preprint arXiv*, 2008, 13611. <https://doi.org/10.48550/arXiv.2008.13611>
- Karpathy, A., Toderici, G., Shetty, S., Leung, T., Sukthankar, R., & Fei-Fei, L. (2014). Large-scale video classification with convolutional neural networks. In *Proceedings of the IEEE Conference on Computer Vision and Pattern Recognition* (pp. 1725–1732). <https://doi.org/10.1109/CVPR.2014.223>
- Klein, P., & Lapeyre, G. (2009). The oceanic vertical pump induced by mesoscale and submesoscale turbulence. *Annual Review of Marine Science*, 1(1), 351–375. <https://doi.org/10.1146/annurev.marine.010908.163704>
- Kleshcheva, T. I., Permyakov, M. S., Salyuk, P. A., & Golik, I. A. (2021). Wavenumber spectra of the chlorophyll “a” concentration and the sea surface temperature in the area of the anticyclonic eddy in the South China Sea. *Journal of Oceanography*, 77(2), 259–267. <https://doi.org/10.1007/s10872-020-00567-1>
- Lévy, M., Ferrari, R., Franks, P. J. S., Martin, A. P., & Rivière, P. (2012). Bringing physics to life at the submesoscale. *Geophysical Research Letters*, 39(14), L14602. <https://doi.org/10.1029/2012gl052756>
- Lin, C. C., & Lau, Y. Y. (1979). Density wave theory of spiral structure of galaxies. *Studies in Applied Mathematics*, 60(2), 97–163. <https://doi.org/10.1002/sapm197960297>
- Ling, F., Luo, J. J., Li, Y., Tang, T., Bai, L., Ouyang, W., & Yamagata, T. (2022). Multi-task machine learning improves multi-seasonal prediction of the Indian Ocean Dipole. *Nature Communications*, 13(1), 7681. <https://doi.org/10.1038/s41467-022-35412-0>

- Liu, F., Tang, S., & Chen, C. (2014). Satellite observations of the small-scale cyclonic eddies in the western South China Sea. *Biogeosciences*, 12(2), 299–305. <https://doi.org/10.1029/2005JC002932>
- Liu, X., & Levine, N. M. (2016). Enhancement of phytoplankton chlorophyll by submesoscale frontal dynamics in the North Pacific Subtropical Gyre. *Geophysical Research Letters*, 43(4), 1651–1659. <https://doi.org/10.1002/2015GL066996>
- Liu, Z., Hu, H., Lin, Y., Yao, Z., Xie, Z., Wei, Y., et al. (2022). Swin transformer v2: Scaling up capacity and resolution. In *Proceedings of the IEEE/CVF Conference on Computer Vision and Pattern Recognition* (pp. 12009–12019). <https://doi.org/10.48550/arXiv.2111.09883>
- Liu, Z., Lin, Y., Cao, Y., Hu, H., Wei, Y., Zhang, Z., et al. (2021). Swin transformer: Hierarchical vision transformer using shifted windows. In *Proceedings of the IEEE/CVF International Conference on Computer Vision* (pp. 10012–10022). <https://doi.org/10.48550/arXiv.2103.14030>
- Mahadevan, A. (2016). The impact of submesoscale physics on primary productivity of plankton. *Annual Review of Marine Science*, 8(1), 161–184. <https://doi.org/10.1146/annurev-marine-010814-015912>
- Maritorena, S., d'Andon, O. H. F., Mangin, A., & Siegel, D. A. (2010). Merged satellite ocean color data products using a bio-optical model: Characteristics, benefits and issues. *Remote Sensing of Environment*, 114(8), 1791–1804. <https://doi.org/10.1016/j.rse.2010.04.002>
- Maritorena, S., & Siegel, D. A. (2005). Consistent merging of satellite ocean color data sets using a bio-optical model. *Remote Sensing of Environment*, 94(4), 429–440. <https://doi.org/10.1016/j.rse.2004.08.014>
- Martin, A. P., & Srokosz, M. A. (2002). Plankton distribution spectra: Inter-size class variability and the relative slopes for phytoplankton and zooplankton. *Geophysical Research Letters*, 29(24), 66–71. <https://doi.org/10.1029/2002GL015117>
- Martínez-Moreno, J., Hogg, A. M., England, M. H., Constantinou, N. C., Kiss, A. E., & Morrison, A. K. (2021). Global changes in oceanic mesoscale currents over the satellite altimetry record. *Nature Climate Change*, 11(5), 397–403. <https://doi.org/10.1038/rs.3.rs-88932/v1>
- McGillicuddy, D. J. (2016). Mechanisms of physical-biological-biogeochemical interaction at the oceanic mesoscale. *Annual Review of Marine Science*, 8(1), 125–159. <https://doi.org/10.1146/annurev-marine-010814-015606>
- McGillicuddy, D. J., Anderson, L. A., Bates, N. R., Bibby, T., Buesseler, K. O., Carlson, C. A., et al. (2007). Eddy/wind interactions stimulate extraordinary mid-ocean plankton blooms. *Science*, 316(5827), 1021–1026. <https://doi.org/10.1126/science.1136256>
- McGillicuddy, D. J., Anderson, L. A., Doney, S. C., & Maltrud, M. E. (2003). Eddy-driven sources and sinks of nutrients in the upper ocean: Results from a 0.1-degree resolution model of the North Atlantic. *Global Biogeochemical Cycles*, 17(2), 1035. <https://doi.org/10.1029/2002GB001987>
- McGillicuddy, D. J., Robinson, A. R., Siegel, D. A., Jannasch, H. W., Johnson, R., Dickey, T. D., et al. (1998). Influence of mesoscale eddies on new production in the Sargasso Sea. *Nature*, 394(6690), 263–266. <https://doi.org/10.1038/28367>
- McWilliams, J. C. (2008). Fluid dynamics at the margin of rotational control. *Environmental Fluid Mechanics*, 8(5–6), 441–449. <https://doi.org/10.1007/S10652-008-9081-8>
- McWilliams, J. C. (2010). A perspective on submesoscale geophysical turbulence. In *IUTAM Symposium on Turbulence in the Atmosphere and Oceans* (pp. 131–141). Springer. https://doi.org/10.1007/978-94-007-0360-5_11
- McWilliams, J. C. (2016). Submesoscale currents in the ocean. *Proceedings of the Royal Society of London*, 472(2189), 20160117. <https://doi.org/10.1098/rspa.2016.0117>
- McWilliams, J. C., & Yavneh, I. (1998). Fluctuation growth and instability associated with a singularity of the balance equations. *Physics of Fluids*, 10(10), 2587–2596. <https://doi.org/10.1063/1.869772>
- Molemaker, M. J., McWilliams, J. C., & Yavneh, I. (2005). Baroclinic instability and loss of balance. *Journal of Physical Oceanography*, 35(9), 1505–1517. <https://doi.org/10.1175/JPO2770.1>
- Montgomery, M. T., & Kallenbach, R. J. (1997). A theory for vortex Rossby waves and its application to spiral bands and intensity changes in hurricanes. *Quarterly Journal of the Royal Meteorological Society*, 123(538), 435–465. <https://doi.org/10.1002/qj.49712353810>
- Munk, W., Armi, L., Fischer, K. W., & Zachariasen, F. (2000). Spirals on the sea. *Proceedings of the Royal Society A*, 456(1997), 1217–1280. <https://doi.org/10.1098/rspa.2000.0560>
- Ni, Q., Zhai, X., Wilson, C., Chen, C., & Chen, D. (2021). Submesoscale eddies in the south China Sea. *Geophysical Research Letters*, 48(6), e2020GL091555. <https://doi.org/10.1029/2020GL091555>
- Nian, R., Cai, Y., Zhang, Z., He, H., Wu, J., Yuan, Q., et al. (2021). The identification and prediction of mesoscale eddy variation via memory in memory with scheduled sampling for sea level anomaly. *Frontiers in Marine Science*, 8, 753942. <https://doi.org/10.3389/fmars.2021.753942>
- Oschlies, A., & Garçon, V. (1998). Eddy-induced enhancement of primary production in a model of the North Atlantic Ocean. *Nature*, 394(6690), 266–269. <https://doi.org/10.1038/28373>
- Ostrovskii, A. G. (1995). Signatures of stirring and mixing in the Japan Sea surface temperature patterns in autumn 1993 and spring 1994. *Geophysical Research Letters*, 22(17), 2357–2360. <https://doi.org/10.1029/95GL02494>
- Park, K. A., & Chung, J. Y. (1999). Spatial and temporal scale variations of sea surface temperature in the East Sea using NOAA/AVHRR data. *Journal of Oceanography*, 55(2), 271–288. <https://doi.org/10.1023/A:1007872709494>
- Pascual, A., Faugere, Y., Larnicol, G., & Traon, P. Y. L. (2006). Improved description of the ocean mesoscale variability by combining four satellite altimeters. *Geophysical Research Letters*, 33(2), L02611. <https://doi.org/10.1029/2006GL026245>
- Pegliasco, C., Deleplace, A., Mason, E., Morrow, R., Faugère, Y., & Dibarboure, G. (2022). META3. 1exp: A new global mesoscale eddy trajectory atlas derived from altimetry. *Earth System Science Data*, 14(3), 1087–1107. <https://doi.org/10.5194/essd-14-1087-2022>
- Pérez, C., Juan, G., & Calil, P. H. R. (2017). Regional turbulence patterns driven by meso- and submesoscale processes in the Caribbean Sea. *Ocean Dynamics*, 67(9), 1217–1230. <https://doi.org/10.1007/s10236-017-1079-7>
- Qiu, B., Chen, S., Klein, P., Wang, J., Torres, H., Fu, L. L., & Menemenlis, D. (2018). Seasonality in transition scale from balanced to unbalanced motions in the World Ocean. *Journal of Physical Oceanography*, 48(3), 591–605. <https://doi.org/10.1175/JPO-D-17-0169.1>
- Qiu, B., Nakano, T., Chen, S., & Klein, P. (2017). Submesoscale transition from geostrophic flows to internal waves in the northwestern Pacific upper ocean. *Nature Communications*, 8(1), 14055. <https://doi.org/10.1038/ncomms14055>
- Quinlan, J. R. (1993). Combining instance-based and model-based learning. In *Proceedings of the Tenth International Conference on Machine Learning* (pp. 236–243). <https://doi.org/10.1162/b978-1-55860-307-3.50037-x>
- Roy, A. G., Navab, N., & Wachinger, C. (2018). Recalibrating fully convolutional networks with spatial and channel “squeeze and excitation” blocks. *IEEE Transactions on Medical Imaging*, 38(2), 540–549. <https://doi.org/10.1109/TMI.2018.2867261>
- Ruder, S. (2016). An overview of gradient descent optimization algorithms. *arxiv preprint arxiv*, 1609, 04747. <https://doi.org/10.48550/arXiv.1609.04747>
- Sandler, M., Howard, A., Zhu, M., Zhmoginov, A., & Chen, L.-C. (2018). Mobilenetv2: Inverted residuals and linear bottlenecks. *CVPR*. <https://doi.org/10.1109/CVPR.2018.00474>
- Sasaki, H., Klein, P., Qiu, B., & Sasai, Y. (2014). Impact of oceanic-scale interactions on the seasonal modulation of ocean dynamics by the atmosphere. *Nature Communications*, 5(1), 5636. <https://doi.org/10.1038/ncomms6636>

- Schubert, R., Gula, J., Greatbatch, R. J., Baschek, B., & Biastoch, A. (2020). The submesoscale kinetic energy cascade: Mesoscale absorption of submesoscale mixed layer eddies and frontal downscale fluxes. *Journal of Physical Oceanography*, 50(9), 2573–2589. <https://doi.org/10.1175/JPO-D-19-0311.1>
- Siegel, D. A., McGillicuddy Jr, D. J., & Fields, E. A. (1999). Mesoscale eddies, satellite altimetry, and new production in the Sargasso Sea. *Journal of Geophysical Research*, 104(C6), 13359–13379. <https://doi.org/10.1029/1999JC900051>
- Smith, R. C., Zhang, X., & Michaelsen, J. (1988). Variability of pigment biomass in the California current system as determined by satellite imagery: I. Spatial variability. *Journal of Geophysical Research*, 93(D9), 10863–10882. <https://doi.org/10.1029/JD093iD09p10883>
- Tan, M., & Le, Q. (2019). Efficientnet: Rethinking model scaling for convolutional neural networks. In *International Conference on Machine Learning* (pp. 6105–6114). PMLR. <https://doi.org/10.48550/arXiv.1905.11946>
- Tan, M., & Le, Q. (2021). Efficientnetv2: Smaller models and faster training. In *International Conference on Machine Learning* (pp. 10096–10106). PMLR. <https://doi.org/10.48550/arXiv.2104.00298>
- Thomas, L. N., Taylor, J. R., Ferrari, R., & Joyce, T. M. (2013). Symmetric instability in the Gulf Stream. *Deep-Sea Research, Part II*, 91, 96–110. <https://doi.org/10.1016/j.dsret.2013.02.025>
- Travers-Smith, H., Giannini, F., Sastri, A. R., & Costa, M. (2021). Validation of non-photochemical quenching corrections for chlorophyll-a measurements aboard ships of opportunity. *Frontiers in Marine Science*, 8, 686750. <https://doi.org/10.3389/fmars.2021.686750>
- Vallis, G. K. (Ed.) (2006). *Atmospheric and Oceanic Fluid Dynamics* (Pembroke, Ont.) (pp. 247–287). Cambridge University Press. <https://doi.org/10.2277/0521849691>
- Vaswani, A., Shazeer, N., Parmar, N., Uszkoreit, J., Jones, L., Gomez, A. N., et al. (2017). Attention is all you need. *Advances in Neural Information Processing Systems*, 30. <https://doi.org/10.48550/arXiv.1706.03762>
- Wang, D. P., Flagg, C. N., Donohue, K., & Rossby, H. T. (2010). Wavenumber spectrum in the Gulf Stream from shipboard ADCP observations and comparison with altimetry measurements. *Journal of Physical Oceanography*, 40(4), 840–844. <https://doi.org/10.1175/2009JPO4330.1>
- Wang, Q., Wu, B., Zhu, P., Li, P., Zuo, W., & Hu, Q. (2020). ECA-Net: Efficient channel attention for deep convolutional neural networks. In *Proceedings of the IEEE/CVF Conference on Computer Vision and Pattern Recognition* (pp. 11534–11542). <https://doi.org/10.1109/CVPR42600.2020.01155>
- Wang, Y., Zhang, H. R., Chai, F., & Yuan, Y. (2018). Impact of mesoscale eddies on chlorophyll variability off the coast of Chile. *PLoS One*, 13(9), e0203598. <https://doi.org/10.1371/journal.pone.0203598>
- Weichman, P. B., & Glazman, R. E. (2002). Spatial variations of a passive tracer in a random wave field. *Journal of Fluid Mechanics*, 453, 263–287. <https://doi.org/10.1017/S0022112001006942>
- Woo, S., Park, J., Lee, J. Y., & Kweon, I. S. (2018). Cbam: Convolutional block attention module. In *Proceedings of the European Conference on Computer Vision (ECCV)* (pp. 3–19). https://doi.org/10.1007/978-3-030-01234-2_1
- Wu, J., Long, K., Wang, F., Qian, C., Li, C., Lin, Z., & Zha, H. (2019). Deep comprehensive correlation mining for image clustering. In *2019 IEEE/CVF International Conference on Computer Vision (ICCV)* (pp. 8150–8159). IEEE. <https://doi.org/10.1109/iccv.2019.00824>
- Wunsch, C. (2007). The past and future ocean circulation from a contemporary perspective. *Ocean Circulation: Mechanisms and Impacts—Past and Future Changes of Meridional Overturning*, 173, 53–74. <https://doi.org/10.1029/173GM06>
- Xu, G., Dong, C., Liu, Y., Gaube, P., & Yang, J. (2019). Chlorophyll rings around ocean eddies in the North Pacific. *Scientific Reports*, 9(1), 2056. <https://doi.org/10.1038/s41598-018-38457-8>
- Zhang, Q., Wu, Y. N., & Zhu, S. C. (2018). Interpretable convolutional neural networks. In *Proceedings of the IEEE Conference on Computer Vision and Pattern Recognition* (pp. 8827–8836). <https://doi.org/10.1109/CVPR.2018.00920>
- Zhang, Z., & Qiu, B. (2018). Evolution of submesoscale ageostrophic motions through the life cycle of oceanic mesoscale eddies. *Geophysical Research Letters*, 45(21), 11–847. <https://doi.org/10.1029/2018GL080399>
- Zhang, Z., & Qiu, B. (2020). Surface chlorophyll enhancement in mesoscale eddies by submesoscale spiral bands. *Geophysical Research Letters*, 47(14), e2020GL088820. <https://doi.org/10.1029/2020GL088820>
- Zhang, Z., Qiu, B., Klein, P., & Travis, S. (2019). The influence of geostrophic strain on oceanic ageostrophic motion and surface chlorophyll. *Nature Communications*, 10(1), 2838. <https://doi.org/10.1038/s41467-019-10883-w>
- Zhao, D., Xu, Y., Zhang, X., & Huang, C. (2021). Global chlorophyll distribution induced by mesoscale eddies. *Remote Sensing of Environment*, 254, 112245. <https://doi.org/10.1016/j.rse.2020.112245>